SEASONAL AND REGIONAL DIFFERENTIATION OF BIO-OPTICAL PROPERTIES WITHIN THE NORTH POLAR ATLANTIC

Malgorzata Stramska[1], Dariusz Stramski[2], Sławomir Kaczmarek[3], David B. Allison[2], and Jill Schwarz[4]

[1]Hancock Institute for Marine Studies, University of Southern California, Los Angeles, California 90089-0371, USA.

[2]Marine Physical Laboratory, Scripps Institution of Oceanography, University of California at San Diego, La Jolla, California 92093-0238, USA.

[3]Institute of Oceanology, Polish Academy of Sciences, Powstancow Warszawy 55, 81-712 Sopot, Poland

[4]Alfred-Wegener-Institut für Polar- und Meeresforschung, Am Handelshafen 12, 27570 Bremerhaven, Germany

Address to be used for business-related correspondence when this paper is in submission/press:
Dr. Malgorzata Stramska
Marine Physical Laboratory
Scripps Institution of Oceanography
University of California, San Diego
La Jolla, CA 92093-0238
Tel: (858) 534 7841
Fax: (858) 534 7641
Email: mstramska@ucsd.edu

Abstract

Using data collected during spring and summer seasons in the north polar Atlantic we examined the variability of the spectral absorption, $a(\lambda)$, and backscattering, $b_b(\lambda)$, coefficients of surface waters and its relation to phytoplankton pigment concentration and composition. For a given chlorophyll *a* concentration (*TChla*), the concentrations of photosynthetic carotenoids (PSC), photoprotective carotenoids (PPC), and total accessory pigments (AP) were consistently lower in spring than in summer. The chlorophyll-specific absorption coefficients of phytoplankton and total particulate matter were also lower in spring, which can be partly attributed to lower proportions of PPC, PSC, and AP in spring. The spring values of the green-to-blue band ratio of the absorption coefficient were higher than the summer ratios. The blue-to-green ratios of backscattering coefficient were also higher in spring. The higher b_b values and lower blue-to-green b_b ratios in summer were likely associated with higher concentrations of detrital particles in summer compared to spring. Because the product of the green-to-blue absorption ratio and the blue-to-green backscattering ratio is a proxy for the blue-to-green ratio of remote-sensing reflectance, we conclude that the performance of ocean color band-ratio algorithms for estimating pigments in the north polar Atlantic is significantly affected by seasonal shifts in the relationships between absorption and *TChla* as well as between backscattering and *TChla*. Intriguingly, however, fairly good estimate of the particulate beam attenuation coefficient at 660 nm (potential measure of total particulate matter or particulate organic carbon concentration) can be obtained by applying a single blue-to-green band-ratio algorithm for both spring and summer seasons.

1. Introduction

Empirical approaches, in which in situ oceanographic measurements are used to relate band ratios of ocean spectral reflectance to surface water properties such as chlorophyll *a* concentration (*Chla*), are an important component of routine processing of ocean color satellite imagery [e.g., *O'Reilly et al*., 1998]. The well-known example is the OC4 (Ocean Chlorophyll 4) empirical algorithm that is used for processing of global satellite data collected with SeaWiFS (Sea-viewing Wide Field-of-view Sensor). This algorithm estimates chlorophyll *a* concentration from a fourth order polynomial by using the maximum band ratio determined as the greatest of the $R_{rs}(443)/R_{rs}(555)$, $R_{rs}(490)/R_{rs}(555)$, or $R_{rs}(510)/R_{rs}(555)$ values [*O'Reilly et al*., 2000]. $R_{rs}(\lambda)$ is the spectral remote-sensing reflectance defined as the ratio of the spectral upwelling water-leaving radiance just above the sea surface to spectral downwelling plane irradiance incident on the sea surface, where λ is a wavelength of light in vacuum.

A basic connection between 2-band algorithms and inherent optical properties (IOPs) of seawater comes from an approximate relation [*Gordon et al.,* 1988]:

$$R_{rs}(\lambda) \sim b_b(\lambda)/a(\lambda) \qquad (1)$$

where $a(\lambda)$ and $b_b(\lambda)$ are the spectral absorption and backscattering coefficients of seawater, respectively. From Equation (1), the reflectance band ratio is approximately equal to the product of backscattering ratio and absorption ratio:

$$R_{rs}(\lambda_1)/R_{rs}(\lambda_2) \approx [b_b(\lambda_1)/b_b(\lambda_2)]\,[a(\lambda_2)/a(\lambda_1)] \qquad (2)$$

which indicates that changes in $R_{rs}(\lambda_1)/R_{rs}(\lambda_2)$ are driven primarily by the variability in spectral ratios of $b_b(\lambda_1)/b_b(\lambda_2)$ and $a(\lambda_2)/a(\lambda_1)$. Therefore, concurrent measurements of $b_b(\lambda)$ and $a(\lambda)$ offer the opportunity to explain how these IOPs affect the general trends and the spread of data in the relationship of chlorophyll *a* concentration versus $R_{rs}(\lambda_1)/R_{rs}(\lambda_2)$ as well as the temporal and geographical variability in this relationship. The $a(\lambda)$ and $b_b(\lambda)$ coefficients are usually partitioned into a few additive components associated with broadly defined categories of seawater constituents [*e.g*., *Mobley*, 1994]:

$$a(\lambda) = a_w(\lambda) + a_p(\lambda) + a_{CDOM}(\lambda) \qquad (3)$$

$$a_p(\lambda) = a_{ph}(\lambda) + a_d(\lambda)$$

$$b_b(\lambda) = b_{bw}(\lambda) + b_{bp}(\lambda)$$

where the subscript w denotes pure seawater, p the total particulate assemblage suspended in water, ph the phytoplankton suspended in water, d the detrital or non-phytoplankton particles (this component in fact includes non-living organic and mineral particles, and heterotrophic organisms), and CDOM the colored dissolved organic matter. The partitioning of IOPs into these components offers an added value for the interpretation of the effects of $b_b(\lambda_1)/b_b(\lambda_2)$ and $a(\lambda_2)/a(\lambda_1)$ on the relationship between *Chla* and $R_{rs}(\lambda_1)/R_{rs}(\lambda_2)$.

A limited amount of appropriate *in situ* data has held back a development of regional bio-optical and ocean color algorithms in the high northern latitude waters, where relatively few experiments with a broad suite of bio-optical measurements have been made so far [*Mitchell*, 1992; *Cota*, 2001; *Sathyendranath et al*., 2001]. Recently, we described bio-optical relationships derived from data collected on R/V Oceania during the summer season (June – August) in the eastern part of north polar Atlantic between Norway and Spitsbergen [*Stramska et al*., 2003]. The main goal of the present study is to compare these previous results with similar relationships established from more recent data collected on R/V Polarstern during the spring season (April-May). These latest data were collected on a ship's transect starting near Spitsbergen and extending west all the way to the vicinity of Greenland. The eastern part of the Polarstern transect overlapped, in part, with the study area investigated earlier during the Oceania summer cruises. We discuss the variability of the spectral absorption and backscattering coefficients of surface waters and the relation between these IOPs and surface chlorophyll *a* concentration in the north polar Atlantic. This analysis provides insights into seasonal and spatial variability of bio-optical properties that are essential to ocean color algorithms for estimating *Chla* from the blue-to-green reflectance ratio within the investigated region.

2. Data and methods

Data were collected in the north polar Atlantic during spring and summer seasons. The spring data were collected in April-May 2003 on R/V Polarstern operated by Alfred Wegener Institute for Polar and Marine Research (AWI) in Germany. The summer data were collected in June-August of 1999 and 2000 during two cruises on R/V Oceania operated by Institute of Oceanology, Polish Academy of Sciences (IOPAS). Whereas the Oceania cruises covered the eastern part of the north polar Atlantic (0^o-20^oE and 70^o-80^oN), the Polarstern transect extended between 10^oE and 16^oW, mostly along 75^oN. The maps showing the location of stations can be found elsewhere [*Stramska et al.*, 2003; *Stramska and Stramski*, 2005]. The data from Polarstern were divided into two subsets. First, a subset #1 includes data from the eastern side of the transect (between Spitsbergen and 0^oE, mostly at 75^oN), and second, a subset #2 includes data from the western side of the transect (between 4^oW and Greenland, mostly at 75^oN). This division is justified by HPLC analysis of phytoplankton pigments, which suggests significant differences in phytoplankton composition on both sides of the transect, as discussed below. In addition, the spring Polarstern data of subset #1 were collected in the geographic area overlapping with some summer stations occupied on the Oceania cruises. This facilitates unambiguous comparison of data for seasonal variability. However, comparisons of all data from Polarstern and Oceania cruises reflect not only seasonal but also spatial variability within the entire study region.

In this study we consider data from stations where we observed no evidence of significant influence of terrestrial material on the optical properties of seawater. Because our interest is on bio-optical relationships relevant to remote sensing of ocean color, we use data representing surface waters only. During the Polarstern cruise in spring, surface waters in the north polar Atlantic were well-mixed or weakly stratified. Therefore we assume that data collected between the surface and a depth of 30 m characterize the surface water properties and can be used for our purposes. In contrast, during the Oceania cruises in summer, surface waters were stratified, so we use data collected only between the surface and 10 m. In this paper, we do not discuss in situ

radiometric measurements. Although such data were collected on Oceania [*Stramska et al*., 2003], the cruise schedule and ice conditions allowed only for a few underwater radiometric measurements from Polarstern, which is not sufficient to make a meaningful comparison of the radiometric data between the cruises.

Methods of our bio-optical measurements that were carried out on R/V Oceania and R/V Polarstern are described in *Stramska et al*. [2003] and *Stramska and Stramski* [2005]. Below is a description of methods of direct relevance to this paper.

2.1. Pigments

For the analysis of phytoplankton pigments, suspended particles were collected by filtration of water samples onto Whatman glass-fiber filters (GF/F) under low vacuum. Three methods were used to measure the concentration of pigments. The spectrophotometric method (UV4-100 spectrophotometer, Unicam, Ltd) was used to estimate chlorophyll *a* concentration (*Chla*) on board the ship during the Oceania cruises in 1999 and in 2000 (77 samples). In this method the optical density (absorbance) of pigment extract in ethanol was measured at 665 nm. After correction for background signal in the near infrared (750 nm), the absorbance was converted to chlorophyll *a* concentration, *Chla*, using the chlorophyll *a*-specific absorption coefficient in 96% ethanol [see *Stramska et al*., 2003 for details]. In addition, pigment samples (31 samples) on the Oceania cruise in 1999 were stored in liquid nitrogen and analyzed with fluorometric (*Chla* and phaeopigments concentrations) and high-performance liquid chromatography (HPLC) methods after the cruise [*Bidigare and Trees*, 2000; *Trees et al.*, 2000a]. Fluorometric and HPLC methods were also used to analyze pigment samples collected on the Polarstern cruise. Here we report on data from the analysis of 76 pigment samples collected in the top 30 m of water on Polarstern. The HPLC analysis provided an estimate of total *Chla* (*TChla*) concentration that was calculated as a sum of chlorophyll *a* and derivatives (chlorophyllide *a*, chlorophyll *a* allomers and epimers). HPLC also provided concentration of various accessory pigments.

The comparison of chlorophyll *a* concentrations obtained with different methods is shown in Figure 1. The correlation of various estimates is quite good. In particular, a good agreement is observed between the spectrophotometric *Chla* and HPLC-derived *TChla* for samples from the Oceania cruise in 1999. Because of this agreement and because we did not carry out HPLC analysis on Oceania in 2000, we will use the spectrophotometric *Chla* estimates as the chlorophyll *a* concentration for both Oceania cruises. When we discuss the HPLC data from Oceania, it will be explicitly indicated. For the Polarstern cruise we will use the HPLC-derived *TChla* estimates for the chlorophyll *a* concentration.

For more detailed comparisons of phytoplankton pigments from HPLC analysis between our data sets, we define three major categories of accessory pigments. The first category, the photosynthetic carotenoids (PSC), includes peridinin (*per*), fucoxanthin (*fuco*), 19'hexanoyloxyfucoxanthin (*hex*), and 19'butaonoyloxyfucoxanthin (*but*). The second category, the photoprotective carotenoids (PPC), consists of diadinoxanthin (*dda*), alloxanthin (*allo*), diatoxanthin (*diato*), zeaxanthin (*zea*), violaxanthin (*viol*), and α- and β-carotenes. The third category, referred to as the total accessory pigments (AP), is defined as the sum of PSC, PPC, chl *b*, and chl *c*.

HPLC analysis of phytoplankton pigments provides data that can be used to characterize broad algal classes present in a water body. One of the problems in the use of HPLC data for describing phytoplankton community structure is the fact that algal groups do not necessarily have unique pigments to allow unambiguous taxonomic identification. Various approaches have been tested over the years to overcome this problem. One of the most successful methods is based on factor analysis developed into a computer program CHEMTAX [*Mackey et al.*, 1996]. This program was originally used to estimate algal class abundance for samples collected between Australia and Antarctica, where the predominant phytoplankton cells in terms of contribution to Chl *a* are relatively large [*Wright et al.*, 1996] and in the western equatorial Pacific where picoplankton dominate [*Mackey, et al.*, 1998]. Comparisons with traditional cell counting techniques supported the results obtained with CHEMTAX for these locations. Other

successful applications of CHEMTAX include studies of phytoplankton community structure in the Canadian Arctic [*Vidussi et al*., 2004] and near Faroe Islands [*Riegman and Kraay*, 2001].

Using our HPLC data we applied CHEMTAX to estimate the contributions of various algal classes to the *TChla* in our study region. As input to the code, CHEMTAX uses the accessory pigment/*TChla* ratios for a number of algal classes. We did not have available information on accessory pigment/*TChla* ratios for phytoplankton classes present in our study region. Therefore we used the pigment fractions shown in Table 1, which are similar to those used recently to examine phytoplankton community structure in the Faroe-Shetland Channel located to the south of our study region [*Riegman and Kraay,* 2001]. These fractions are in general agreement with other data found in the literature [*Jeffrey and Wright*, 1997]. The fractions given in Table 1 were iteratively modified by CHEMTAX to minimize the sum of squared differences between the observed and calculated pigment concentrations. Because pigment ratios are known to vary with environmental growth conditions (light, nutrients, temperature), we carried out separate calculations for data collected on Oceania and Polarstern cruises to reveal possible seasonal and regional differences. In addition, because our initial CHEMTAX runs suggested different phytoplankton composition at the eastern (data subset #1) and western (data subset #2) parts of the Polarstern transect, independent CHEMTAX runs were made for each of these Polarstern data subsets.

The HPLC data were also used to estimate proportions of phytoplankton present in broad size groups using the method developed by *Vidussi et al.* [2001]. According to this method, if the total diagnostic pigments (DP) are defined as the sum of Chl *b*, *zea*, *allo*, *but*, *hex*, *fuco*, and *per*, then the relative contribution to *TChla* by picoplankton (< 2 μm), nanoplankton (2-20 μm) and microplankton (> 20 μm) can be estimated from the following relationships:

Picoplankton (%) = (*zea* + Chl *b*) · 100/DP

Nanoplankton (%) = (*allo* + *but* + *hex*) · 100/DP

Microplankton (%) = (*fuco* +*per*) · 100/DP

where all pigment concentrations are in mg m^{-3}. Derived in this way phytoplankton size fractions present some limitations [*Vidussi et al.*, 2001]. These limitations result from the facts that certain pigments are present in more than one taxonomic group and that the same phytoplankton taxa can be generally present in different size classes. Nevertheless, to first approximation, we can use this tool to test whether there are significant differences in size structure of phytoplankton populations within the north polar Atlantic.

2.2. Inherent optical properties

In situ vertical profiles of IOPs and physical properties of seawater were measured with a multisensor datalogger system that consisted of the SeaBird Sealogger 25 and SeaBird temperature, conductivity, and pressure sensors, Hydroscat-6 backscattering sensor (442, 470, 555, 589, 620, and 671 nm, HobiLabs, Inc.), and two c-Star beam transmissometers (488 and 660 nm; WetLabs, Inc). We processed the Hydroscat-6 data with the Hydrosoft software (version 2.6 of December 2002, HobiLabs, Inc.), which includes corrections suggested by *Boss and Pegau* [2001]. Because the c-Star transmissometer data were occasionally unavailable, we consistently used a standard correction built-in the Hydrosoft software to account for the light attenuation effects. We verified that the use of correction based on actual beam attenuation measurements instead of the standard correction generally yielded the $b_b(\lambda)$ values higher by a few percent but the blue-to-green ratios of b_b were nearly the same (to within 2% in the extreme cases). Therefore, the choice of attenuation correction method for determining b_b does not affect main conclusions from our analysis. Our final $b_b(\lambda)$ values at Hydroscat-6 wavebands were used to fit a power function, $b_b(\lambda) \sim \lambda^{-\gamma}$, which describes the spectral shape of $b_b(\lambda)$ spectrum. The $b_b(\lambda)$ values at wavelengths corresponding to nominal center wavelengths of SeaWiFS bands were then obtained from this function.

During processing of optical data, all profiles were first carefully inspected for quality, for example for the presence of possible noise in the near-surface data. Doubtful or noisy data were removed from the analysis. Typically we did not consider data acquired within the top 2 or 3

meters of the ocean. The remaining data were averaged into 2-m bins to provide final depth profiles. Surface IOPs were approximated as the averages for the uppermost bin. The relationships for *Chla* versus $b_b(\lambda)$ and *Chla* vs. $c_p(660)$ were obtained by matching *Chla* estimates from discrete water samples and the IOPs measured at corresponding depths. The time difference between the collection of discrete water samples and acquisition of in situ optical data was usually less than an hour.

The spectral absorption coefficient of particulate matter, $a_p(\lambda)$, was derived from filter-pad measurements using a dual-beam UV4-100 spectrophotometer (Unicam, Ltd). First, an appropriate volume of seawater (0.5 – 2 L depending on particle concentration in water) was filtered onto a 25-mm glass-fiber filter (GF/F). Next, the absorption spectrum of particles, $a_p(\lambda)$, retained on a filter was determined using the transmittance-reflectance (T-R) spectrophotometric method [*Tassan and Ferrari,* 1995 a, b]. Transmittance and reflectance were measured between 380 and 750 nm with a 1 nm interval. Correction for pathlength amplification factor (β) was made using the following expression [Kaczmarek et al., 2003]:

$$OD_s = 0.592\ OD_f^2 + 0.4\ OD_f$$

where OD_s is the optical density (absorbance) of particle suspension with no β effect and OD_f is the measured optical density of particles on the filter.

The absorption coefficient of non-phytoplankton (detritus) particles, $a_d(\lambda)$, was determined with another run of transmittance and reflectance measurements after bleaching the filter with sodium hypochlorite [*Ferrari and Tassan*, 1999]. Because it was recently shown that oceanic particles generally do not absorb significantly in the near infrared spectral region [*Babin and Stramski*, 2002], the final estimates of $a_p(\lambda)$ and $a_d(\lambda)$ were derived after subtracting the measured values of a_p and a_d averaged between 740 and 750 nm. Finally, the phytoplankton absorption coefficient, $a_{ph}(\lambda)$, was calculated as a difference between $a_p(\lambda)$ and $a_d(\lambda)$. During the Oceania cruises the absorption measurements were made on freshly collected samples on board the ship. The a_p samples from the Polarstern cruise were stored in liquid nitrogen and analyzed in the laboratory after the cruise.

The absorption data from the Oceania cruises presented in our previous paper [*Stramska et al*., 2003] were calculated from filter-pad measurements performed in the transmittance (T) configuration [*e.g*., *Mitchell et al*., 2000]. However, because the reflectance (R) measurements were also made on Oceania, we now recalculated the absorption spectra using the T-R algorithm. In the blue-green spectral region the differences between the 'old' and 'new' $a_p(\lambda)$ estimates from Oceania cruises are generally within a few percent. We note that the T-R method may be superior to T-method. The T-R method accounts (albeit still not perfectly) for wavelength-dependent scattering error and the pathlength amplification factor applied in the T-R method is less variable than in the T-method [*Ferrari and Tassan*, 1999; *Tassan and Ferrari,* 2002]. The absorption data from the Oceania and Polarstern cruises discussed in this paper were determined in the same way with the T-R method.

3. Results and discussion

3.1. Pigments

Surface chl *a* concentrations varied from 0.2 to 0.8 mg m^{-3} and from 0.2 to 10 mg m^{-3} in the eastern and western parts of the Polarstern transect respectively. High chl *a* concentrations in the west indicate the presence of a well-developed phytoplankton bloom, while comparatively low chl *a* concentrations in the east suggest a pre-bloom or early bloom phase. Fairly high chl *a* concentrations observed during Oceania cruises (0.2 - 3 mg m^{-3}) suggest that phytoplankton growth in the eastern part of the region has been supported throughout the summer season, most likely due to periodical replenishment of nutrients by mixing events caused by episodic storms.

CHEMTAX pigment analysis revealed some differences in the composition of phytoplankton community between our data sets, that is between the summer data set from Oceania and two spring subsets (eastern and western) from Polarstern. Note that as explained in Mackey et al. [1998] the phytoplankton classes derived from CHEMTAX do not correspond exactly to conventional taxa but are representative of typical pigment composition.

In our data sets, diatoms and prymnesiophyceae generally dominated the phytoplankton biomass expressed in terms of *TChla*. At nearly all stations, diatoms and prymnesiophyceae combined together contributed more than 50% of *TChla* (Figure 2). The dominance of diatoms was most pronounced in the western part of the Polarstern transect, where we observed an active development of spring phytoplankton bloom. Stations located in the eastern part of the Polarstern transect, which likely represent a pre-bloom situation, were dominated by prymnesiophyceae (~ 30% of *TChla*). Other phytoplankton groups with significant contribution to *TChla* in the eastern part of Polarstern transect were chrysophyceae and prasinophyceae (each ~ 20% of *TChla*). The stations visited in summer by Oceania were dominated either by diatoms or by prymnesiophyceae (on average each group represented somewhat less than 30% of *TChla*). Cryptophyceae and chrysophyceae each contributed on average a little more than 10% of *TChla* during Oceania and Polarstern cruises. The summer stations were characterized by somewhat more abundant populations of dinophyceae and cyanophyceae and less abundant population of prasinophyceae than the spring stations, but the contribution to *TChla* of each of these groups was on average low (well below 10%). The chlorphyceae were present in a small percentage of the total phytoplankton community. Examples of the final pigment ratios estimated with CHEMTAX are shown in Figure 3. The high ratios for *fuco* and *hex* for diatoms and prymnesiophyceae in Oceania data set are particularly noticeable.

In Figure 4 the concentrations of three pigment groups (PPC, PSC, and AP) are plotted as a function of *TChla*. Each pigment group is well correlated with *TChla*. The most important observation is that the concentrations of PPC, PSC, and AP for a given *TChla* were consistently higher in summer (Oceania data set) than in spring (both for the eastern and western data from Polarstern). For example, the concentrations of AP for a given *TChla* were, on average, about two times higher in summer than in spring. The parameter values for the best fit of the linear regression on log-transformed data for total accessory pigments versus *TChla* are compared in Figure 4c with similar global relationship established by *Trees et al.* [2000b]. In contrast to our study, *Trees et al*. included phaeopigments in the accessory pigments. However, their results of

statistical analysis were not significantly affected by phaeopigments because of low concentrations of these pigments in their data set. Our data are within the range reported by *Trees et al*. However, most of our data points from the summer season are above the global relationship of *Trees et al*. and most of our spring data are below that relationship.

Figure 5 shows proportions of pico-, nano-, and microphytoplankton derived from the method of *Vidussi et al.* [2001]. Picoplankton was always the least important of the size classes in terms of contribution to *TChla*. The lowest and the highest relative contributions to total phytoplankton biomass from microphytoplankton were detected in the eastern and the western parts of the Polarstern transect, respectively. Generally, the differences in phytoplankton size structure seem to be more pronounced between the eastern and western sections of the Polarstern transect, than between the averages for the entire Polarstern and Oceania data sets (the averages for combined Polarstern data are not shown in Figure 5).

3.2. Phytoplankton and total particulate absorption

Phytoplankton were the dominant component of particulate absorption for both the Polarstern and Oceania data sets as shown by the relationships between $a_{ph}(\lambda)$ and $a_p(\lambda)$ for the blue wavebands, 442 and 490 nm in Figure 6. In spring, phytoplankton contributed, on average, 76% and 79 % to a_p at 442 and 490, respectively. In summer this contribution was about 71% and 72%, respectively. This indicates that the percent contribution of detritus to absorption in the blue was generally somewhat higher in summer than in spring. In the green spectral band centered at 555 nm, phytoplankton contributed, on average, about 64% to the total a_p in both the spring and summer seasons (not shown).

Figure 7 shows representative examples of $a_{ph}(\lambda)$ normalized to chlorophyll *a* concentration, *i.e*., the chlorophyll-specific absorption coefficient of phytoplankton, $a^*_{ph}(\lambda)$. This figure illustrates a trend of decrease of $a^*_{ph}(\lambda)$ with an increase of chl *a* concentration. Similar trend was observed in larger data sets that combined observations from various regions [*Bricaud et al*., 1995; *Babin et al*., 2003] and it was attributed to increasing pigment packaging, changes in

species composition, and changes in proportions of accessory pigments from oligotrophic to eutrophic waters. Importantly, Figure 7 also shows a significant difference between the relatively high $a^*_{ph}(\lambda)$ observed in summer on the Oceania cruises and low values in spring on the Polarstern cruise. Note that both the eastern and the western parts of the Polarstern transect were characterized by lower $a^*_{ph}(\lambda)$ than the summer values from the Oceania cruises. This indicates a seasonal variation in $a^*_{ph}(\lambda)$. This variation can be, to a large degree, attributed to higher proportions of PPC, PSC, and AP in summer than in spring populations of phytoplankton (*see* Figure 4). This trend of seasonal change in the ratio of accessory pigments to *TChla* is consistent with similar seasonal patterns in pigment composition described by others [*Babin et al*., 2003].

The difference between the spring and summer data of $a_{ph}^*(\lambda)$ can be also partly attributed to the pigment package effect. The package effect reduces the a_{ph}^* values and flattens the $a_{ph}^*(\lambda)$ spectrum. This effect increases with an increase of average cell size and intracellular concentration of pigments within phytoplankton cells [*Morel and Bricaud*, 1981]. The package effect is often estimated by comparison of $a_{ph}^*(675)$ with the pigment absorption of chlorophyll *a* in solution because accessory pigments have relatively small influence on a_{ph}^* in the red absorption band of chlorophyll *a*. Because $a_{ph}^*(675)$ was, on average, 0.17 and 0.27 m^2 (mg chl $a)^{-1}$ for Polarstern and Oceania data sets, the package effect appears to be stronger for the spring phytoplankton populations than for the summer populations. Based on the differences in phytoplankton size structure shown in Figure 5, one could also expect a regional differentiation in the package effect between the eastern and western Polarstern data. In the western part of the Polarstern transect the package effect could have been higher than in the eastern part due to a higher contribution of large microphytoplankton cells to the total phytoplankton biomass as indicated in Figure 5. However, no clear differences in the magnitude of a_{ph}^* are observed between the two Polarstern data subsets in Figure 7. We note that variations in the concentration of chlorophyll *b* and phaeopigments also contribute to $a_{ph}^*(675)$, which may confound the interpretation of the package effect.

Because both the eastern and western subsets of Polarstern data show significantly lower $a^*_{ph}(\lambda)$ than the Oceania data, from now on we will discuss and compare the differences in the absorption between the two main seasonal data sets, that is the summer data set (from Oceania) and the spring data set (*i.e.*, combined eastern and western Polarstern data). We will, however, keep on distinguishing the eastern and western Polarstern data points on most graphs. The differences in absorption between the summer and spring data sets are reflected in Figure 8, which shows the relationships for a_{ph} and a_p at 442 and 555 nm vs. chl *a* concentration. The a_{ph} values for a given chl *a* concentration are consistently lower in spring than summer (Figure 8a). Similarly, the a_p values are generally lower in spring than in summer (Figure 8b). Therefore, similarly to a_{ph}*, the chlorophyll *a*-specific absorption coefficient for total particulate matter, a_p*, is lower in spring than in summer. Figure 8 also compares our absorption data with relationships obtained by *Bricaud et al*. [1995; 1998] for a large data set from various regions. Whereas our summer data tend to be higher than the values predicted with the *Bricaud et al*. regression lines, our spring data tend to be lower than these lines.

Differentiation between our spring and summer data sets from the north polar Atlantic is also obvious if we compare the green-to-blue spectral ratios of the absorption coefficient vs. pigment concentration (Figures 9, 10, and 11). If we consider a sum of the absorption contributions of pure water and phytoplankton, a_{w+ph}, there is a good correlation between the a_{w+ph} band ratio and chl *a* concentration if each of our data sets is considered separately. However, for the same chl *a* concentration, the spring data show consistently higher values of a_{w+ph} band ratio than the summer data (Figure 9). Similar behavior of the a_{w+ph} band ratio is observed when plotted vs. total pigment concentration (*i.e.*, vs. *TChla* + AP) although in this case the seasonal differences are somewhat smaller (Figure 10). When we consider a sum of absorption contributions of pure water and total particulate matter, a_{w+p}, the seasonal differences in the a_{w+p} band ratio at any given chl *a* concentration are even more pronounced than in the case of the a_{w+ph} band ratio (Figure 11). The seasonal difference in the ratio of *TChla* to accessory pigments (Figure 4)

appears to be a significant cause for the seasonal differences in the data shown in Figures 9 and 11.

The behavior of the green-to-blue absorption ratio has important implications for ocean color algorithms that are based on the blue-to-green reflectance ratio (*see* Equation 2). It is important to realize that our absorption band ratios in Figure 11 do not fully represent the absorption term on the right-hand side of Equation 2. This is obviously because we have omitted the contribution of colored dissolved organic matter, $a_{CDOM}(\lambda)$, to the total absorption coefficient, $a(\lambda)$. Unfortunately, $a_{CDOM}(\lambda)$ was not measured during our experiments. However, the contribution of $a_{CDOM}(\lambda)$ to $a(\lambda)$ was suggested to be quite small for our summer data set [*Stramska et al*., 2003]. For open waters within the investigated region, we expect that $a_{CDOM}(\lambda)$ would not play a significant role in spring either because the estimates of DOM concentration during the Polarstern cruise were relatively low (*Schwarz et al.*, submitted). Therefore, it is reasonable to assume that the green-to-blue ratio of the total absorption coefficient would behave qualitatively in a similar manner as the green-to-blue ratio of the absorption coefficient by pure seawater and particles displayed in Figure 11.

3.3. Backscattering

The backscattering coefficients $b_b(\lambda)$ at 442 and 555 nm for any given chl *a* concentration are generally lower for the Polarstern than for the Oceania data set, although the scatter of data points is large, especially for the Oceania data set (Figure 12a). In spring the contribution of particles to total $b_b(555)$ (*i.e*., the sum of particulate and molecular backscattering at 555 nm) was usually between 40 and 50%, and exceeded 60% only at a few stations. In summer this contribution at most stations was between 70 and 90%. The spectral dependency of $b_b(\lambda)$ was also different for the two data sets (Figure 12b). Assuming that $b_b(\lambda)$ has the wavelength dependence defined by:

$$b_b(\lambda) = [b_{bw}(555) + b_{bp}(555)](\lambda/555)^{-\gamma} \qquad (4a)$$

the slope γ for the spring data is best described by the following equation:

$$\gamma = 0.026\, b_b(555)^{-0.750} \quad (4b)$$

and for the summer data by:

$$\gamma = 0.067\, b_b(555)^{-0.572} \quad (4c)$$

The changes in γ result primarily from variability in relative contributions of water molecules and particles to the total backscattering [*Morel and Gentili*, 1991]. Pure water backscattering coefficient, $b_{bw}(\lambda)$, is characterized by strong wavelength dependency, $b_{bw}(\lambda) \sim \lambda^{-4.32}$ [*Morel*, 1974]. The wavelength dependency of particulate backscattering coefficient, $b_{bp}(\lambda)$, for natural populations of marine particles is usually less pronounced, and $b_{bp}(\lambda) \sim \lambda^{-1}$ is sometimes assumed in models [*Carder et al*., 1999]. In general, however, $b_{bp}(\lambda)$ depends on the variability in concentration, size distribution, and composition of particulate assemblages, and these sources of backscattering variability are not yet well understood [*Stramski et al.*, 2004]. Note that in Figure 12b the steepest slopes γ close the value of 4 or even slightly exceeding 4 were observed in clear waters with low $b_b(555)$ (corresponding to relatively low chl *a* concentration) in the spring season. In these cases the water molecules dominated the total backscattering coefficient.

According to Equation (2), the blue-to-green backscattering ratio is one of the important factors driving the reflectance band ratio that is used in chlorophyll algorithms. Figure 13 shows $b_b(442)/b_b(555)$ and $b_b(490)/b_b(555)$ plotted as a function of chl *a* concentration for the spring and summer data sets. For each of the data sets, chl *a* concentration changes nearly 30-fold but the range of b_b ratios is relatively small, that is a factor of 1.6 and 1.3 for $b_b(442)/b_b(555)$ and $b_b(490)/b_b(555)$, respectively. Most importantly, however, these backscattering ratios are significantly higher for the spring data than the summer data, which is consistent with generally higher spectral slopes in the spring (*see* Figure 12b). The results in Figure 13 have important implications for the seasonal differentiation of the band ratio algorithms for estimating chl *a* concentration. The differences in the b_b band ratios shown in Figure 13 will reinforce the effect of absorption because the green-to-blue absorption ratio (Figure 11) was also higher in spring than in summer.

Without detailed data of particle size distribution and composition, the interpretation of the observed differences in backscattering would be mostly speculative. It was, however, hypothesized that non-living particles (mostly from the small size range < 1 μm) can dominate the particulate backscattering in most open ocean situations in the absence of intense phytoplankton blooms [*Morel and Ahn*, 1991; *Stramski and Kiefer*, 1991; *Stramski et al.*, 2004]. Our absorption data suggest that non-living particles were more abundant in summer than in the spring season because we observed higher total particulate and higher detrital absorption coefficients as well as higher POC concentrations for a given chl *a* concentration [not shown here] during summer. Therefore, higher b_b values and lower blue-to-green b_b ratios observed in summer can perhaps be associated with higher concentrations of detrital particles observed in summer compared to spring. The backscattering ratio of particles defined as $b_{bp}(\lambda)/b_p(\lambda)$ where $b_p(\lambda)$ is $c_p(\lambda) - a_p(\lambda)$, is sometimes used as a source of general information about particle sizes and/or composition [see *Stramski et al.*, 2004 and references therein]. We found that at $\lambda = 488$ nm, the b_{bp}/b_p values in summer were either lower or similar to the values measured in spring (Figure 14a). In contrast, at $\lambda = 660$ nm, the b_{bp}/b_p values in summer were either higher or similar to the values measured in spring (Figure 14b). We show the results for these two wavelengths because the beam attenuation $c_p(\lambda)$ was measured at these two bands only. One conclusion from Figure 14 is that the b_{bp}/b_p values are relatively small (usually less than 0.01), which suggests that particulate assemblages in the investigated region are dominated by organic particles with low refractive index. Another important conclusion from Figure 14 is that the particulate assemblages in spring were characterized by much stronger wavelength dependency of the backscattering ratio than in the summer season. In spring, $b_{bp}(488)/b_p(488)$ is generally greater than 0.004 - 0.005 but $b_{bp}(660)/b_p(660)$ is always smaller than 0.004 and often times less than 0.002. For the summer data set, the spectral dependency of the b_{bp}/b_p ratio is not so obvious or well pronounced. These differences in the spectral behavior of b_{bp}/b_p suggest that particles in summer could have been, on average, smaller than particles in spring [*Morel and Bricaud*, 1986; *Stramski et al*. 2001]. In addition, the overall particle concentration in summer was probably, on

average, higher than in spring, as suggested by higher beam attenuation in summer (*see* section 3.4 below). The possible seasonal differences in particle concentration and size distribution would support generally higher backscattering per unit chlorophyll *a* concentration in summer than in spring shown in Figure 12.

3.4. Particulate beam attenuation and single scattering albedo

The relationship between the particulate beam attenuation coefficient at 660 nm, $c_p(660)$, and chlorophyll *a* concentration shows a shift between the spring and summer data (Figure 15). For any chl *a* concentration, $c_p(660)$ is generally higher during the summer season than in spring. This shift is qualitatively similar to that discussed above with regard to the particulate absorption and backscattering coefficients. The seasonal shifts in the IOP vs. chl *a* concentration relationships appear to be related to increased roles of accessory pigments and/or detrital particles in summer. The variability in particulate absorption, especially by accessory pigments, is expected to have minor influence on the particulate beam attenuation at 660 nm. Therefore the observed seasonal shift in $c_p(660)$ vs. chl *a* concentration is most likely due to an increased detrital scattering in summer.

Given significant seasonal differences in several bio-optical relationships discussed above, it is remarkable that a range of single scattering albedo values, $\omega_{op}(\lambda)$, for suspended particulate matter is about the same for the spring and summer seasons (Figure 16). The $\omega_{op}(\lambda)$ values calculated as $b_p(\lambda)/c_p(\lambda)$ where $b_p(\lambda) = c_p(\lambda) - a_p(\lambda)$, characterize the particles in terms of the relative roles of scattering and absorption in the beam attenuation process. Figure 16 indicates that scattering dominates the beam attenuation both in the blue band at 488 nm and in the red band at 660 nm. Figure 16 also suggests that $\omega_{op}(\lambda)$ at any given phytoplankton biomass (chl *a* concentration) shows no clear systematic differences between the spring and summer seasons.

One of the most striking results is that the green-to-blue absorption ratio follows one consistent pattern as a function of $c_p(660)$ regardless of whether the data were collected in spring or summer (Figure 17). This is not the case for the blue-to-green backscattering ratio, which

shows a seasonal shift if plotted vs. $c_p(660)$ (Figure 18). This shift is qualitatively similar to that observed for the IOP band ratios plotted as a function of Chl *a* (*see* Figures 11 and 13).

3.5. Implications for ocean color band-ratio algorithms

We now illustrate variations of chl *a* concentration, total pigments (= *TChla*+AP), $c_p(660)$, and $a_{ph}(442)$ as a function of the product of the backscattering ratio $b_b(442)/b_b(555)$ and the absorption ratio $a_{w+p}(555)/a_{w+p}(442)$ (Figure 19). Similar illustration but for the 490 nm and 555 nm bands is shown in Figure 20. Because the product of the IOP band ratios is a proxy for the blue-to-green ratios of remote-sensing reflectance R_{rs} (*see* Equation 2), these figures show potential variability in the empirical band-ratio algorithms for estimating pigments, phytoplankton absorption, and particulate beam attenuation in the north polar Atlantic. We recall a limitation of these results due to the fact that the presented absorption ratios do not include a contribution from colored dissolved organic matter. Nevertheless, we expect that the main effect of CDOM would be to shift slightly the presented patterns of data points to the left without much effect on the differentiation between the spring and summer data sets.

The results in Figures 19 and 20 are straightforward consequences of the relationships discussed in the previous sections. First, it is clear that chl *a* concentration estimated from the blue-to-green band-ratio of ocean color signal in the north polar Atlantic will be significantly affected by seasonal shifts in the relationships between absorption and chl *a* as well as between backscattering and chl *a*. The effects of absorption and backscattering reinforce each other in a way that the seasonal difference in the band-ratio chlorophyll algorithm will be quite large. For example, Figures 19a and 20a indicate that the relationship for the spring season will predict chl *a* concentration that is higher by a factor of 4-6 compared to that predicted from the summer relationship. Second, Figures 19b and 20b suggest that seasonal differences in the band-ratio algorithm for estimating total pigments (*TChla* + AP) will be smaller than those for estimating just chl *a* concentration. Still, estimating total pigments will require a seasonal approach as our results suggest that the spring relationship would predict *TChla* + AP that is higher by a factor 2-

4 than the summer estimates. Third, it appears that ignoring seasonal differentiation and using just one single algorithm for estimating phytoplankton absorption at 442 nm from the blue-to-green reflectance ratio will have a much smaller effect on the accuracy of the resulting product compared to pigments (Figures 19c and 20c). The differences in spring and summer estimates of $a_{ph}(442)$ are within a factor of 2-2.5.

Finally, perhaps the most striking and unexpected result is that a single band-ratio algorithm based on data pooled together from both spring and summer seasons can provide a fairly good estimate of the particulate beam attenuation coefficient at 660 nm (Figures 19d and 20d). Note that the relationships of $c_p(660)$ versus the product of IOP band-ratio (that is, versus a proxy for blue-to-green ratio of reflectance) are the only relationships in Figures 19 and 20, which show no clear seasonal shift between the spring and summer data. This result is intriguing and rather difficult to interpret in simple terms because the variability in the band-ratio of reflectance in the investigated region is driven largely by the variability in absorption and to a smaller extent by backscattering [*e.g.*, *Stramska et al*., 2003] whereas the variability in the beam attenuation in red part of the spectrum at 660 nm is expected to be driven primarily by particle scattering, especially forward scattering. Although we have already shown that the relatively robust relationship between $c_p(660)$ and the blue-to-green reflectance ratio in the north polar Atlantic can be used as an intermediate step in the regional algorithm for estimating particulate organic carbon from ocean color observations [*Stramska and Stramski*, 2005], further research is needed to examine whether this type of relationship exhibits a similar degree of robustness in other regions of the worlds' ocean.

Acknowledgments. Financial support for this research was provided by NASA Grants NAG5-6512, NAG5-6466, NAG5-12396, and NAG5-12397 (awarded to M.S. and D.S.), and by Institute of Oceanology, Polish Academy of Sciences (S.K). Field work on R/V Oceania in 1999 and 2000 was supported by the Polish Academy of Sciences. Field work on R/V Polarstern in 2003 was supported by the Alfred Wegener Institute in Germany. We are grateful to Chief

Scientists, G. Kattner, J. Piechura, and W. Walczowski for accommodating our bio-optical measurements on the cruises. We thank the scientists, officers, and crews of R/V Oceania and R/V Polarstern for invaluable assistance in the collection of field data and logistical support.

REFERENCES

Babin, M., and D. Stramski (2002), Light absorption by aquatic particles in the near-infrared spectral region, *Limnol. Oceanogr*., 47, 911-915.

Babin, M., D. Stramski, G. M. Ferrari, H. Claustre, A. Bricaud, G. Obolenski, and N. Hoepffner (2003), Variations in the light absorption coefficients of phytoplankton, nonalgal particles, and dissolved organic matter in coastal waters around Europe, *J. Geophys. Res*., 108 (C7), 3211, doi:10.1029/2001JC000882.

Bidigare, R., and C. C. Trees (2000), HPLC phytoplankton pigments: sampling, laboratory methods, and quality procedures assurance, *NASA Tech. Memo*., 2000-209966, 154-161.

Boss, E., W. S. Pegau (2001), The relationship of light scattering at an angle in the backward direction to the backscattering coefficient, *Appl. Opt.*, 40, 5503-5507.

Bricaud A., M. Babin, A. Morel, and H. Claustre (1995), Variability in the chlorophyll-specific absorption coefficients of natural phytoplankton: Analysis and parameterization, *J. Geophys. Res*., 100, 13321-13332.

Bricaud A., A. Morel, M. Babin, K. Allali, H. Claustre (1998), Variations of light absorption by suspended particles with chlorophyll *a* concentration in oceanic (case 1) waters: Analysis and implications for bio-optical models, *J. Geophys. Res*., 103, 31033-31044.

Carder, K. L., F. R. Chen, Z. P. Lee, and S. K. Hawes (1999), Semianalytic Moderate-Resolution Imaging Spectrometer algorithms for chlorophyll *a* and absorption with bio-optical domains based on nitrate-depletion temperatures, *J. Geophys. Res*., 104, 5403-5421.

Cota, G. F. (2001), Remote sensing of ocean color in the Arctic: Algorithm development and comparative validation, *NASA Tech. Memo*., 2001-209976, 65-70.

Ferrari G. M., and S. Tassan (1999), A method using chemical oxidation to remove light absorption by phytoplankton pigments, *J. Phycol*., 35, 1090-1098.

Gordon, H. R., O. B. Brown, R. H. Evans, J. W. Brown, R. C. Smith, K. S. Baker, and D. K. Clark (1988), A semianalytical radiance model of ocean color, *J. Geophys. Res*., 93, 10909-10924.

Jeffrey, S. W., S.W. Wright (1997), Qualitative and quantitative analysis of SCOR reference algal cultures, In: S.W. Jeffrey, R.F.C. Mantoura, S.W.Wright (Eds.), *Phytoplankton Pigments in Oceanography: Guidelines to Modern Methods*, SCOR-UNESCO, Paris pp. 343-360.

Kaczmarek, S., D. Stramski, M. Stramska (2003), The new pathlength amplification factor investigation, Baltic Sea Science Congress, Helsinki, Abstract Publication, 149.

Mackey, D. J., H.W. Higgins, M. D. Mackey, and D. Holdsworth (1998), Algal class abundances in the western equatorial Pacific: Estimation form HPLC measurements of chloroplast pigments using CHEMTAX, *Deep-Sea Res. I*, 45, 1441-1468.

Mackey, M. D., D.J. Mackey, H.W. Higgins, S.W. Wright (1996), CHEMTAX – a program for estimating class abundances from chemical markers: application to HPLC measurements of phytoplankton, *Mar. Ecol. Prog. Ser*., 144, 265-283.

Mitchell, B. G. (1992), Predictive bio-optical relationships for polar oceans and marginal ice zones, *J. Mar. Syst*., 3, 91-105.

Mitchell, B. G., A. Bricaud, K. Carder, J. Cleveland, G. Ferrari, R. Gould, M. Kahru, M. Kishino, H. Maske, T. Moisan, L. Moore, N. Nelson, D. Phinney, R. Reynolds, H. Sosik, D. Stramski, S. Tassan, C. Trees, A. Weidemann, J. Wieland, and A. Vodacek (2000), Determination of spectral absorption coefficients of particles, dissolved material and phytoplankton for discrete water samples, *NASA Tech. Memo*., 2000-209966, 125-153.

Mobley C. D. (1994), *Light and Water. Radiative Transfer in Natural Waters*, 592 pp., Academic Press, San Diego.

Morel A. (1974), Optical properties of pure water and pure seawater, In: N.G. Jerlov and E. Steeman-Nielsen (Eds.), *Optical Aspects of Oceanography*, pp.1-24, New York, Academic Press.

Morel A., and Y. H. Ahn (1991), Optics of heterotrophic nanoflagellates and cilates - a tentative assessment of their scattering role in oceanic waters compared to those of bacterial and algal cells, *J. Mar. Res*., 49, 177-202.

Morel, A., and A. Bricaud, 1981, Theoretical results concerning light absorption in a discrete medium, and application to specific absorption of phytoplankton, *Deep Sea Res., Part A*, 28, 1375-1393.

Morel, A., and B. Gentili (1991), Diffuse reflectance of oceanic waters: its dependence on sun angle as influenced by the molecular scattering contribution, *Appl. Opt.,* 30, 4427-4438.

O'Reilly, J. E, S. Maritorena, B. G. Mitchell, D. A. Siegel, K. L. Carder, S. A. Garver, M. Kahru, and C. R. McClain (1998), Ocean color chlorophyll algorithms for SeaWiFS, *J. Geophys. Res., 103*, 24,937 - 24,953.

O'Reilly, J. E., S. Maritorena, D. A. Siegel, M. C. O'Brien, D. Toole, B. G. Mitchell, M. Kahru, F. P. Chavez, P. Strutton, G. F. Cota, S. B. Hooker, C. R. McClain, K. L. Carder, F. Müller-Karger, L. Harding, A. Magnuson, D. Phinney, G. F. Moore, J. Aiken, K. R. Arrigo, R. Letelier, and M. Culver (2000), Ocean color chlorophyll *a* algorithms for SeaWiFS, OC2 and OC4: Version 4, *NASA Tech. Memo, 2000-206892, vol. 11*, 9-27.

Riegman R., and G.W. Kraay (2001), Phytoplankton community structure derived from HPLC analysis of pigments in the Faroe-Shetland Channel during summer 1999: the distribution of taxonomic groups in relation to physical/chemical conditions in the photic zone, *J. Plankton Res.*, 32, 191-205.

Sathyendranath, S., G. Cota, V. Stuart, H. Maass, and T. Platt (2001), Remote sensing of phytoplankton pigments: a comparison of empirical and theoretical approaches, *Int. J. Remote Sens.*, 22, 249-273.

Schwarz, J. N., M. Stramska, G. Budeus, E. F. I. Fer, G. Kattner, and Ch. Lorenzen, Observations of the spring bloom in the Greenland Sea, 2003, (2005), Submitted to Elsevier Science.

Stramska M., and D. Stramski (2005), Variability of particulate carbon concentration in the north polar Atlantic based on SeaWiFS ocean color observations, *J. Geophys. Res.* in press.

Stramska M., D. Stramski, R. Hapter, S. Kaczmarek, and J. Ston (2003), Bio-optical relationships and ocean color algorithms for the north polar regions if the Atlantic, *J. Geophys. Res., 108* (C5), 3143, doi:1029/2001JC001195.

Stramski D., and D. A. Kiefer (1991), Light-scattering by microorganisms in the open ocean, *Prog. Oceanogr*., 28, 343-383.

Stramski D., E. Boss, D. Bogucki, and K.J. Voss (2004), The role of seawater constituents in light backscattering in the ocean, *Prog. Oceanogr.*, 61, 27-56.

Tassan S., and G. M. Ferrari (1995a), An alternative approach to absorption measurements of aquatic particles retained on filters, *Limnol. Oceanogr.*, 40, 1358-1368.

Tassan S., and G. M. Ferrari (1995b), Proposal for the measurement of backward and total scattering by mineral particles suspended in water, *Appl. Opt*., 34, 8345-8353.

Tassan S., Ferrari G. M., (2002), A sensitivity analysis of the "Transmittance-Reflectance" method for measuring light absorption by aquatic particles, J. Plankton Res., 24(8), 757-774.

Trees, C. C., R. R. Bidigare, D. M. Karl, and L. Van Heukelem (2000a), Fluorometric chlorophyll *a*: Sampling, laboratory methods, and data analysis protocols, *NASA Tech. Memo*., 2000-209966, 162-169.

Trees, C. C., D. K. Clark, R. R. Bidigare, M. E. Ondrusek, and J. L. Mueller (2000b), Accessory pigments versus chlorophyll a concentration within the euphotic zone: A ubiquitous relationship, *Limnol. Oceanogr*., 45, 1130-1143.

Vidussi F., H. Claustre, B. Manca, A. Luchetta, and J.-C. Marty (2001), Phytoplankton pigment distribution in relation to the upper thermocline circulation in the eastern Mediterranean Sea during winter, *J. Geophys. Res*., 106, 19939-29956.

Vidussi F., S. Roy, C. Lovejoy, M. Gammelgaard, H.A. Thomsen, B. Booth, J-E. Tremblay, and B. Mostajir (2004), Spatial and temporal variability of the phytoplankton community structure in the North Water Polynya, investigated using pigment biomarkers, *Can. J. Fish. Aquat. Sci*., 61, 2038-2052.

Wright, S. W., D. P Thomas, H. J. Marchant, H. W. Higgins, M. D. Mackey, D. J. Mackey (1996), Analysis of phytoplankton of the Australian sector of the Southern Ocean: comparisons of microscopy and size-frequency data with interpretations of pigment HPLC data using the CHEMTAX matrix factorization program, *Mar. Ecol. Prog. Ser.,* 144, 285-298.

Table 1. Input matrix with pigment fractions used in CHEMTAX pigment analysis. Abbreviations: Chlorophyll (*chl*), peridinin *(per*), 19'butaonoyloxyfucoxanthin (*but*), fucoxanthin (*fuco*), 19'hexanoyloxyfucoxanthin (*hex*), prasinoxanthin (*pras*), neoxanthin (*neo*), violaxanthin (*viola*), diadinoxanthin (*dda*), alloxanthin (*allo*), lutein, (*lut*), zeaxanthin (*zea*).

	chla	*chlb*	*chlc*3	*per*	*but*	*fuco*	*hex*	*pras*	*neo*	*viol*	*dda*	*allo*	*lut*	*zea*
diatoms	0.541	0	0	0	0	0.291	0	0	0	0	0.034	0	0	0
cyano-phyceae	0.615	0	0	0	0	0	0	0	0	0	0	0	0	0.301
dino-phycaea	0.308	0	0	0.328	0	0	0.118	0	0	0	0.074	0	0	0
prymnesio-phyceae	0.439	0	0.13	0	0.004	0.132	0.187	0	0	0	0.024	0	0	0
chryso-phyceae	0.471	0	0.057	0	0.214	0.159	0	0	0	0	0.027	0	0	0
chloro-phyceae	0.563	0.233	0	0	0	0	0	0	0.032	0.026	0	0	0.105	0
crypto-hyceae	0.75	0	0	0	0	0	0	0	0	0	0	0.154	0	0
prasino-phyceae	0.442	0.363	0	0	0	0	0	0.063	0.043	0.014	0	0	0	0

Figure Captions

Figure 1. Comparison of the total chlorophyll *a* concentration from HPLC analysis (*TChla*) and chlorophyll *a* concentration estimated with fluorometric and spectrophotometric (*Chla*) methods.

Figure 2. Average contribution (%) of various algal classes to total chlorophyll *a* concentration (*TChla*). Polarstern data are shown as averages for the eastern and western sections of the transect, as explained in the text. Abbreviations: diatoms (*diat*), prasinophyceae (*prasin*), dinophyceae (*dino*), cyanophyceae (*cyan*), chlorophyceae (*chlor*), cryptophyceae (*crypt*), prymnesiophyceae (*prymn*), chrysophyceae (*chrys*).

Figure 3. Final marker pigment : *TChla* ratios for selected algal classes, as calculated by CHEMTAX.

Figure 4. Concentrations of (a) photoprotective carotenoids (PPC, see text for definitions), (b) photosynthetic carotenoids (PSC), and (c) total accessory pigments (AP) as a function of total chlorophyll *a* concentration (*TChla*). The results of linear regressions performed on log-transformed data are shown as solid lines. The regression line for AP versus *TChla* from *Trees et al*. [2000b] is shown as the dashed line.

Figure 5. Approximate contribution (%) of algal size classes to *TChla*. Abbreviations: micro - microphytoplankton; nano - nanophytoplankton, pico - picophytoplankton.

Figure 6. The absorption coefficient of phytoplankton, a_{ph}, as a function of the total particulate absorption coefficient, a_p, at 442 and 490 nm. Data from the Oceania and Polarstern cruises are indicated by solid and open symbols respectively.
The least-squares fits for Polarstern data:

$a_{ph}(442) = 0.85\ a_p(442) - 0.002$; $r^2 = 0.99$; $n = 73$

$a_{ph}(490) = 0.85\ a_p(490) - 0.001$; $r^2 = 0.99$; $n = 73$

The least-squares fits for Oceania data:

$a_{ph}(442) = 0.83\ a_p(442) - 0.008$; $r^2 = 0.93$; $n = 77$

$a_{ph}(490) = 0.86\ a_p(490) - 0.005$; $r^2 = 0.92$; $n = 77$

Figure 7. Examples of the spectra of chlorophyll-specific absorption coefficient of phytoplankton, a^*_{ph}, measured at various chlorophyll *a* concentrations during Polarstern and Oceania cruises. Each example spectrum represents an average obtained from averaging absorption spectra from 3 to 5 stations for the range of chlorophyll *a* concentrations (in mg m^{-3}) as indicated on each graph.

Figure 8. The coefficients of (a) phytoplankton absorption, $a_{ph}(\lambda)$, (b) total particulate absorption, $a_p(\lambda)$, plotted as a function of chlorophyll *a* concentration for the two wavelengths, 442 and 555 nm. Our data from Oceania and Polarstern are compared with regression lines from *Bricaud et al*. [1995] and *Bricaud et al*. [1998] shown as solid and dashed lines for 442 and 555 nm respectively.

Figure 9. The absorption ratios $a_{w+ph}(555)/a_{w+ph}(442)$ and $a_{w+ph}(555)/a_{w+ph}(490)$ as a function of *TChla* from HPLC analysis. Data from Oceania and Polarstern are shown as solid and open symbols respectively.

The least-squares fits for Polarstern data:

$a_{w+ph}(555)/a_{w+ph}(442) = 1.848\ TChla^{-0.541}$; $r^2 = 0.93$; $n = 73$

$a_{w+ph}(555)/a_{w+ph}(490) = 1.931\ TChla^{-0.307}$; $r^2 = 0.91$; $n = 73$

The least-squares fits for Oceania data:

$a_{w+ph}(555)/a_{w+ph}(442) = 1.036\ TChla^{-0.687}$; $r^2 = 0.91$; $n = 31$

$a_{w+ph}(555)/a_{w+ph}(490) = 1.221\ TChla^{-0.512}$; $r^2 = 0.89$; $n = 31$

Figure 10. The absorption ratios $a_{w+ph}(555)/a_{w+ph}(442)$ and $a_{w+ph}(555)/a_{w+ph}(490)$ as a function of the sum of *TChla* and AP. Data from Oceania and Polarstern are shown as solid and open symbols respectively.

The least-squares fits for Polarstern data:

$a_{w+ph}(555)/a_{w+ph}(442) = 2.590\ (TChla + \mathrm{AP})^{-0.575}$; $r^2 = 0.94$; $n = 73$

$a_{w+ph}(555)/a_{w+ph}(490) = 2.338\ (TChla + \mathrm{AP})^{-0.326}$; $r^2 = 0.92$; $n = 73$

The least-squares fits for Oceania data:

$a_{w+ph}(555)/a_{w+ph}(442) = 1.924\ (TChla + \mathrm{AP})^{-0.676}$; $r^2 = 0.93$; $n = 31$

$a_{w+ph}(555)/a_{w+ph}(490) = 1.945\ (TChla + \mathrm{AP})^{-0.512}$; $r^2 = 0.93$; $n = 31$

Figure 11. The absorption ratios $a_{w+p}(555)/a_{w+p}(442)$ and $a_{w+p}(555)/a_{w+p}(490)$ as a function of chlorophyll *a* concentration.

The least-squares fits for Polarstern data:

$a_{w+p}(555)/a_{w+p}(442) = 1.58\ TChla^{-0.51}$; $r^2 = 0.90$; $n = 73$

$a_{w+p}(555)/a_{w+p}(490) = 1.77\ TChla^{-0.3}$; $r^2 = 0.88$; $n = 73$

The least-squares fits for Oceania data:

$a_{w+p}(555)/a_{w+p}(442) = 0.83\ Chla^{-0.554}$; $r^2 = 0.82$; $n = 71$

$a_{w+p}(555)/a_{w+p}(490) = 1.04\ Chla^{-0.427}$; $r^2 = 0.79$; $n = 71$

Figure 12. (a) The total backscattering coefficient b_b at 442 and 555 nm versus chlorophyll *a* concentration. (b) Slope parameter γ from equation 4 versus the total backscattering coefficient b_b at 555 nm.

The least-squares fit for Polarstern data:

$\gamma = 0.026\ b_b(555)^{-0.750}$; $r^2 = 0.95$; $n = 60$

The least-squares fit for Oceania data:

$\gamma = 0.067\ b_b\ (555)^{-0.572}$; $r^2 = 0.80$; $n = 73$

Figure 13. The backscattering ratios $b_b(442)/b_b(555)$ and $b_b(490)/b_b(555)$ as a function of chlorophyll *a* concentration.

The least-squares fits for Polarstern data:

$b_b(442)/b_b(555) = 2.152\ TChla^{-0.093}$; $r^2 = 0.70$; $n = 60$

$b_b(490)/b_b(555) = 1.526\ TChla^{-0.052}$; $r^2 = 0.73$; $n = 60$

The least-squares fits for Oceania data:

$b_b(442)/b_b(555) = 1.583\ Chla^{-0.106}$; $r^2 = 0.66$; n = 73

$b_b(490)/b_b(555) = 1.289\ Chla^{-0.058}$; $r^2 = 0.66$; n = 73

Figure 14. The particulate backscattering ratios (a) $b_{bp}(488)/b_p(488)$ and (b) $b_{bp}(660)/b_p(660)$ as a function of chlorophyll *a* concentration.

Figure 15. Relationships between the particulate beam attenuation coefficient at 660 nm, $c_p(660)$, and chlorophyll *a* concentration.

The least-squares fit for Polarstern data:

$c_p(660) = 0.1995\ TChla^{0.4995}$; $r^2 = 0.89$; $n = 42$

The least-squares fits for Oceania data:

$c_p(660) = 0.4244\ Chla^{0.5282}$; $r^2 = 0.72$; $n = 60$

Figure 16. The single scattering albedo of particles, $\omega_{op}(488)$ and $\omega_{op}(660)$, as a function of chlorophyll *a* concentration.

Figure 17. The absorption ratios $a_{w+p}(555)/a_{w+p}(442)$ and $a_{w+p}(555)/a_{w+p}(490)$ as a function of the particulate beam attenuation coefficient, $c_p(660)$.

The least-squares fits for Polarstern and Oceania data combined together:

$a_{w+p}(555)/a_{w+p}(442) = 0.6144\ c_p(660)^{-0.6441}$; $r^2 = 0.90$; $n = 102$

$a_{w+p}(555)/a_{w+p}(490) = 0.3834\ c_p(660)^{-0.9065}$; $r^2 = 0.89$; $n = 102$

Figure 18. The backscattering ratios $b_b(442)/b_b(555)$ and $b_b(490)/b_b(555)$ as a function of the particulate beam attenuation coefficient, $c_p(660)$.

The least-squares fits for Polarstern data:

$b_b(442)/b_b(555) = 1.570\ c_p(660)^{-0.198}$; $r^2 = 0.91$; $n = 42$

$b_b(490)/b_b(555) = 1.283\ c_p(660)^{-0.109}$; $r^2 = 0.91$; $n = 42$

The least-squares fits for Oceania data:

$b_b(442)/b_b(555) = 1.426\ c_p(660)^{-0.127}$; $r^2 = 0.47$; $n = 60$

$b_b(490)/b_b(555) = 1.217\ c_p(660)^{-0.070}$; $r^2 = 0.47$; $n = 60$

Figure 19. Relationships for (a) chlorophyll *a* concentration versus the product of the backscattering ratio and the absorption ratio, $R = [b_b(442)/b_b(555)]\ [a_{w+p}(555)/a_{w+p}(442)]$. This product is an approximation of the blue-to-green ratio of remote-sensing reflectance (see Eq. 1).

The least-squares fit for Polarstern data:

$TChla = 6.2517\ R^{-1.5349}$; $r^2 = 0.87$; $n = 42$

The least-squares fit for Oceania data:

$Chla = 1.4437\ R^{-1.32}$; $r^2 = 0.83$; $n = 60$

(b) As in (a) but for the sum of *TChla* and AP.

The least-squares fit for Polarstern data:

$(TChla + \mathrm{AP}) = 10.135\ R^{-1.4456}$; $r^2 = 0.88$; $n = 42$

The least-squares fit for Oceania data:

$(TChla + \mathrm{AP}) = 4.0145\ R^{-1.384}$; $r^2 = 0.85$; $n = 26$

(c) As in (a) but for the phytoplankton absorption coefficient at 442 nm, $a_{ph}(442)$.

The least-squares fit for Polarstern data:

$a_{ph}(442) = 0.1467\ R^{-1.3449}$; $r^2 = 0.98$; $n = 42$

The least-squares fit for Oceania data:

$a_{ph}(442) = 0.0885\ R^{-1.3257}$; $r^2 = 0.93$; $n = 50$

(d) As in (a) but for the particulate beam attenuation coefficient at 660 nm, $c_p(660)$.

The least-squares fits for Polarstern and Oceania data combined together:

$c_p(660) = 0.5227\ R^{-0.784}$; $r^2 = 0.93$; $n = 92$

Figure 20. Relationships for (a) chlorophyll *a* concentration versus the product of the backscattering ratio and the absorption ratio, $R = [b_b(490)/b_b(555)]\ [a_{w+p}(555)/a_{w+p}(490)]$. This product is an approximation of the blue-to-green ratio of remote-sensing reflectance (see Eq. 1).

The least-squares fit for Polarstern data:

$TChla = 12.318\ R^{-2.5844}$; $r^2 = 0.86$; $n = 42$

The least-squares fit for Oceania data:

$Chla = 1.6766\ R^{-1.7356}$; $r^2 = 0.79$; $n = 60$

(b) As in (a) but for the sum of *TChla* and AP.

The least-squares fit for Polarstern data:

$(TChla + AP) = 19.189\ R^{-2.4337}$; $r^2 = 0.86$; n = 42

The least-squares fit for Oceania data:

$(TChla + AP) = 5.1763\ R^{-1.9446}$; $r^2 = 0.85$; $n = 26$

(c) As in (a) but for the phytoplankton absorption coefficient at 442 nm, $a_{ph}(442)$.

The least-squares fit for Polarstern data:

$a_{ph}(442) = 0.2696\ R^{-2.2766}$; $r^2 = 0.97$; $n = 42$

The least-squares fit for Oceania data:

$a_{ph}(442) = 0.1054\ R^{-1.8014}$; $r^2 = 0.95$; $n = 50$

(d) As in (a) but for the particulate beam attenuation coefficient at 660 nm, $c_p(660)$.

The least-squares fits for Polarstern and Oceania data combined together:

$c_p(660) = 0.5999\ R^{-1.1475}$; $r^2 = 0.92$; $n = 92$

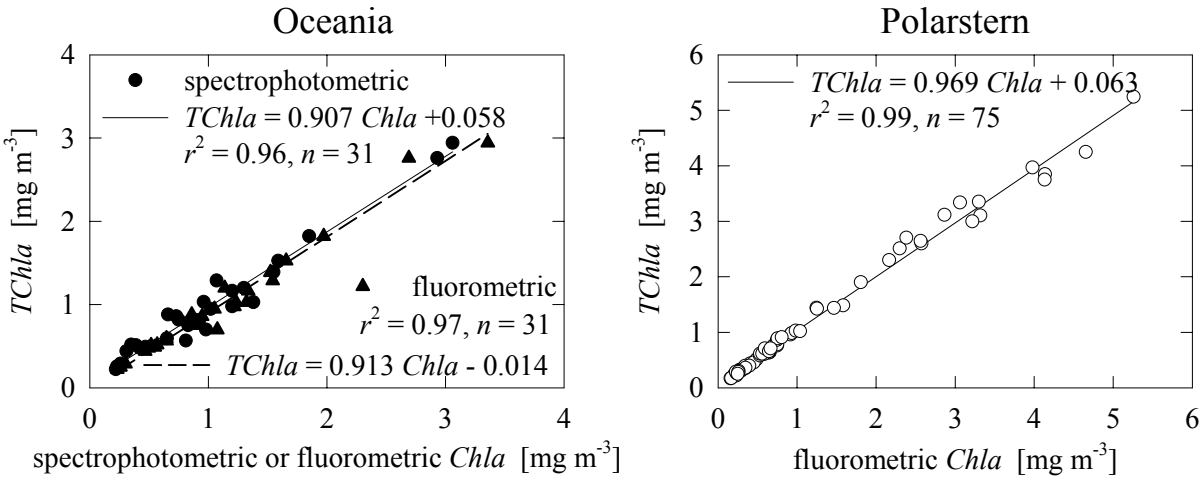

Figure 1. Comparison of the total chlorophyll *a* concentration from HPLC analysis (*TChla*) and chlorophyll *a* concentration estimated with fluorometric and spectrophotometric (*Chla*) methods.

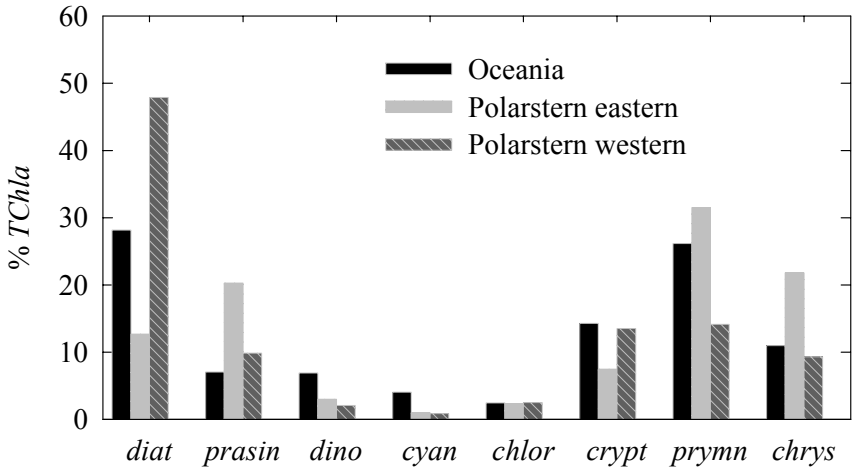

Figure 2. Average contribution (%) of various algal classes to total chlorophyll *a* concentration (*TChla*). Polarstern data are shown as averages for the eastern and western sections of the transect, as explained in the text. Abbreviations: diatoms (*diat*), prasinophyceae (*prasin*), dinophyceae (*dino*), cyanophyceae (*cyan*), chlorophyceae (*chlor*), cryptophyceae (*crypt*), prymnesiophyceae (*prymn*), chrysophyceae (*chrys*).

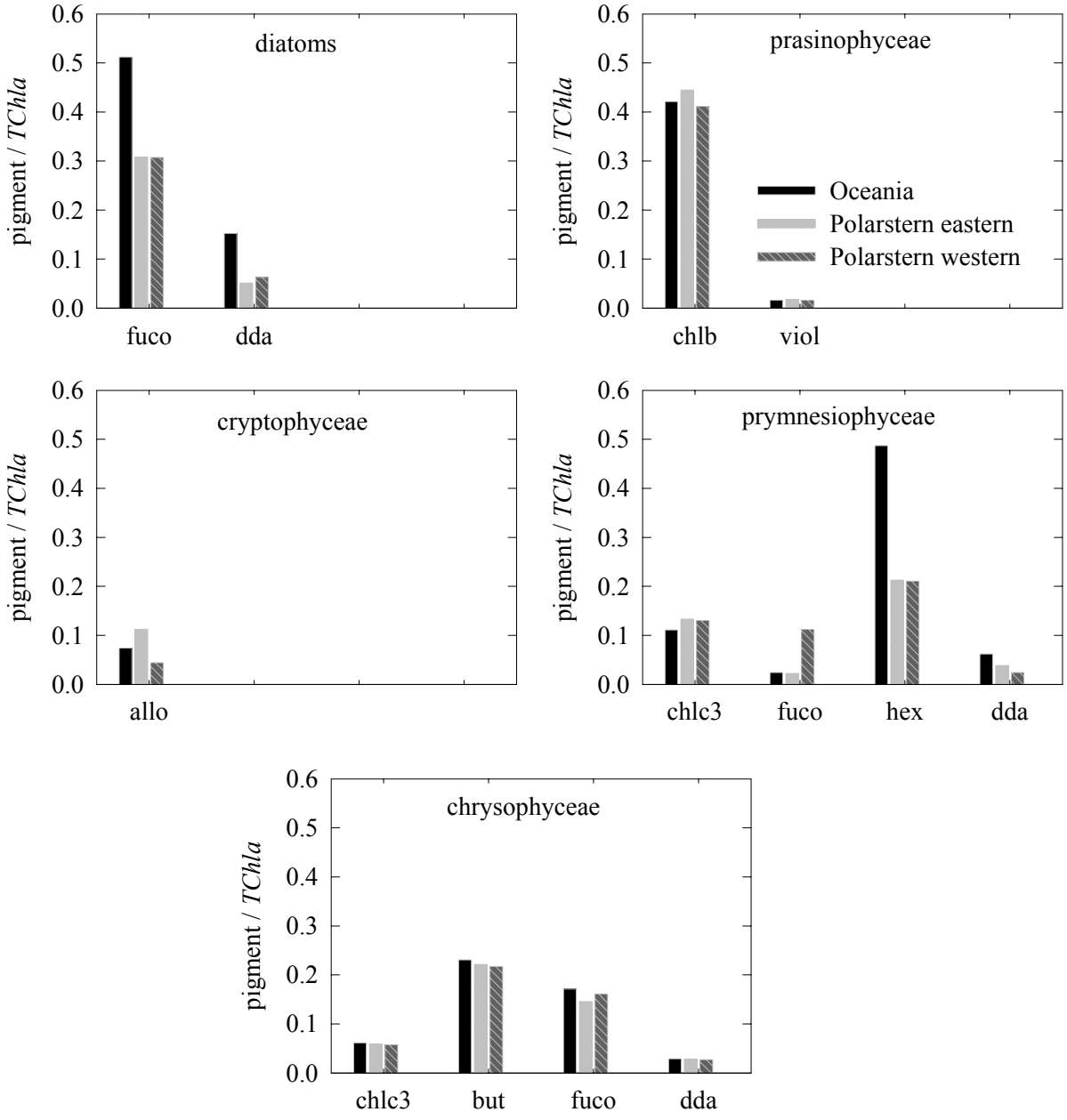

Figure 3. Final marker pigment : *TChla* ratios for selected algal classes, as calculated by CHEMTAX.

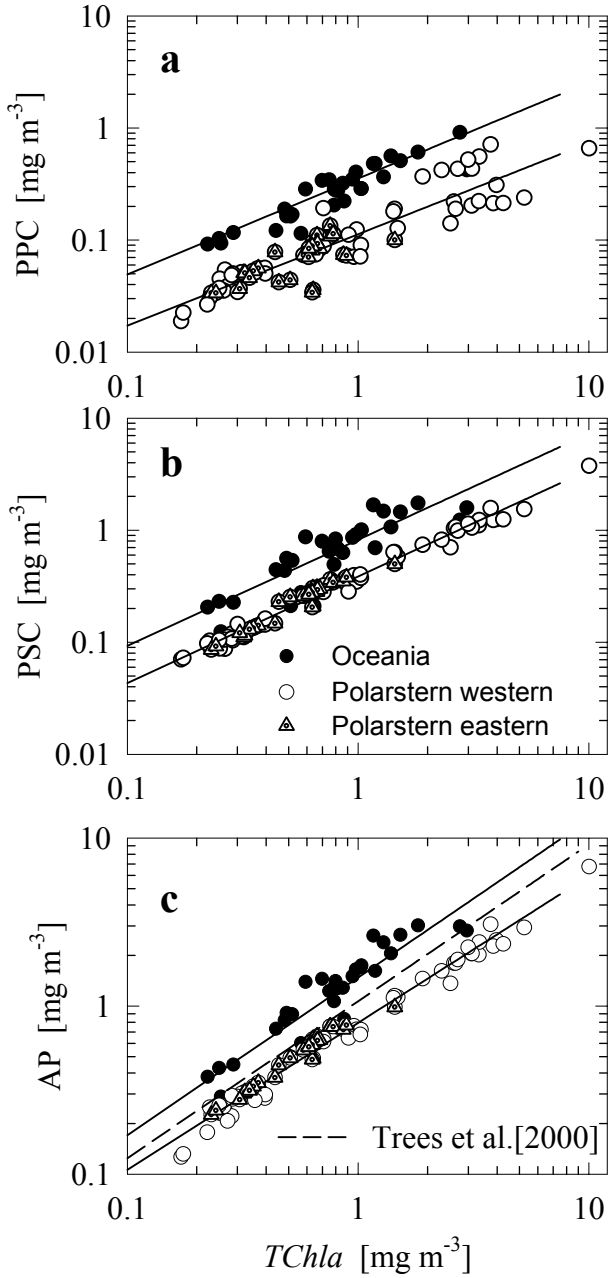

Polarstern all data
log(PPC) = 0.816 log(*TChla*) - 0.948
r^2 = 0.84, *n* = 75

Oceania
log(PPC) = 0.857 log(*TChla*) - 0.450
r^2 = 0.84, *n* = 31

Polarstern all data
log(PSC) = 0.951 log(*TChla*) - 0.413
r^2 = 0.96, *n* = 75

Oceania
log(PSC) = 0.947 log(*TChla*) - 0.085
r^2 = 0.78, *n* = 31

Polarstern all data
log(AP) = 0.874 log(*TChla*) - 0.10
r^2 = 0.98, *n* = 75

Oceania
log(AP) = 0.939 log(*TChla*) +0.170
r^2 = 0.87, *n* = 31

Trees et al. [2000b]
log (AP) = 0.934 log (*TChla*)+0.028
r^2 = 0.95, *n*= 5617

Figure 4. Concentrations of (a) photoprotective carotenoids (PPC, see text for definitions), (b) photosynthetic carotenoids (PSC), and (c) total accessory pigments (AP) as a function of total chlorophyll *a* concentration (*TChla*). The results of linear regressions performed on log-transformed data are shown as solid lines. The regression line for AP versus *TChla* from *Trees et al*. [2000b] is shown as the dashed line.

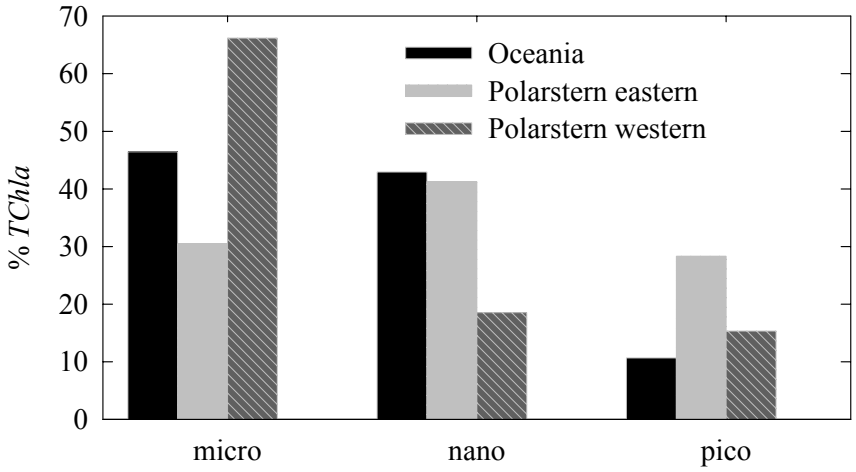

Figure 5. Approximate contribution (%) of algal size classes to total chlorophyll *a* concentration (*TChla*). Abbreviations: micro - microphytoplankton; nano - nanophytoplankton, pico - picophytoplankton.

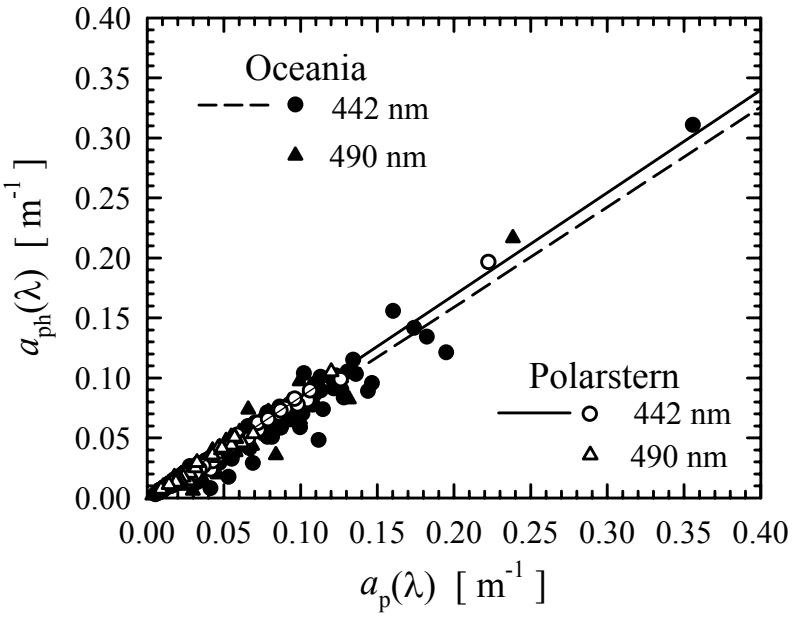

Figure 6. The absorption coefficient of phytoplankton, a_{ph}, as a function of the total particulate absorption coefficient, a_p, at 442 and 490 nm. Data from the Oceania and Polarstern cruises are indicated by solid and open symbols respectively.

The least-squares fits for Polarstern data:

$a_{ph}(442) = 0.85\ a_p(442) - 0.002$; $r^2 = 0.99$; $n = 73$

$a_{ph}(490) = 0.85\ a_p(490) - 0.001$; $r^2 = 0.99$; $n = 73$

The least-squares fits for Oceania data:

$a_{ph}(442) = 0.83\ a_p(442) - 0.008$; $r^2 = 0.93$; $n = 77$

$a_{ph}(490) = 0.86\ a_p(490) - 0.005$; $r^2 = 0.92$; $n = 77$

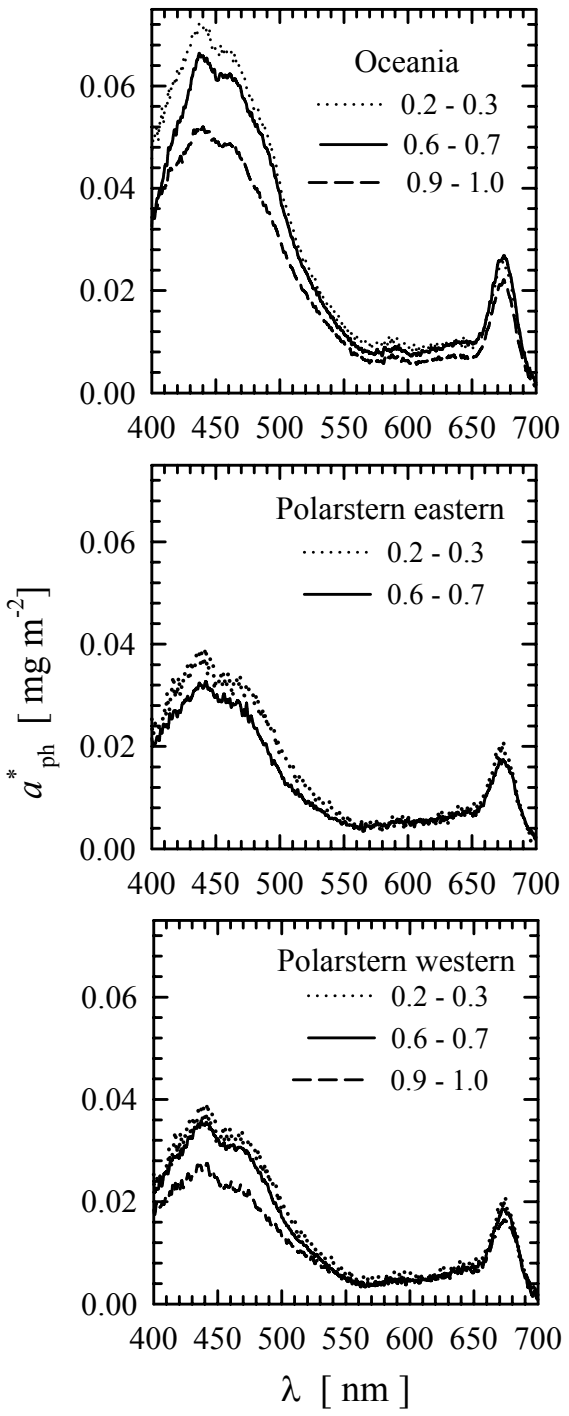

Figure 7. Examples of the spectra of chlorophyll-specific absorption coefficient of phytoplankton, a^*_{ph}, measured at various chlorophyll *a* concentrations during Polarstern and Oceania cruises. Each example spectrum represents an average obtained from averaging absorption spectra from 3 to 5 stations for the range of chlorophyll *a* concentrations (in mg m^{-3}) as indicated on each graph.

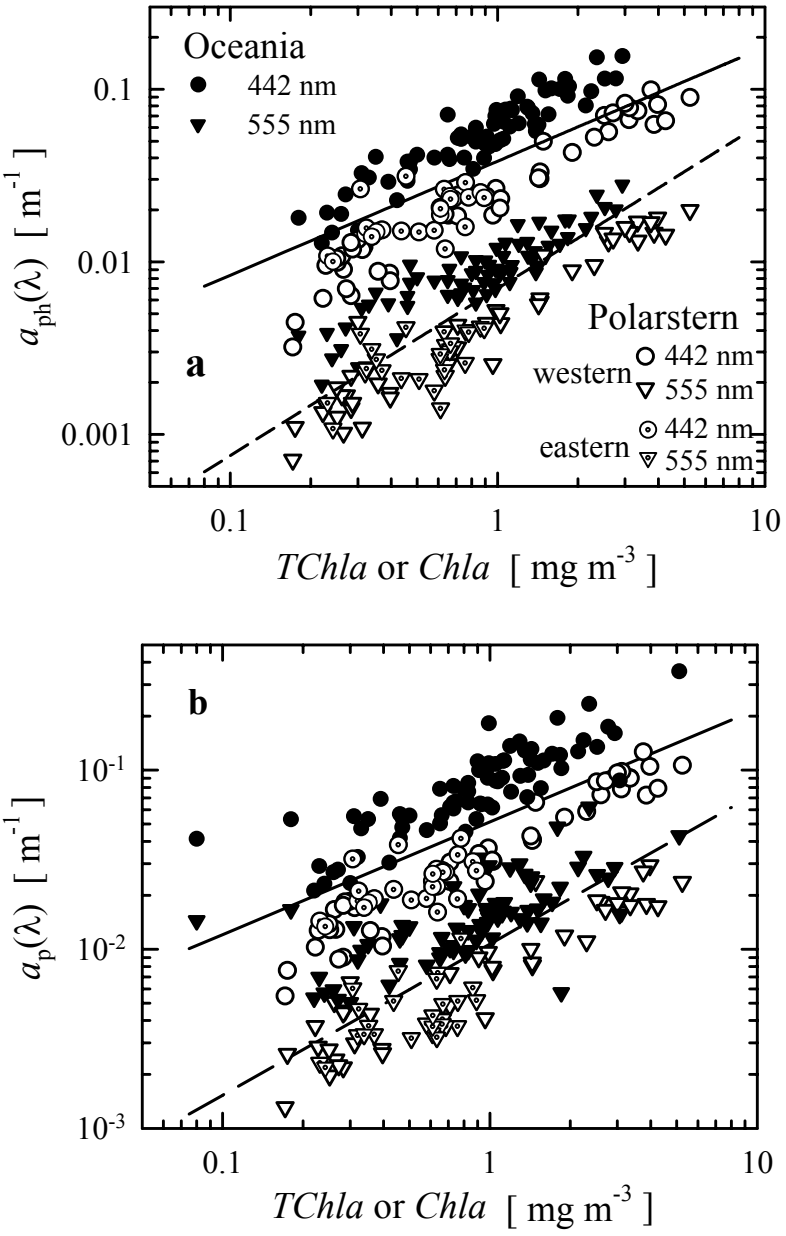

Figure 8. The coefficients of (a) phytoplankton absorption, $a_{ph}(\lambda)$, (b) total particulate absorption, $a_p(\lambda)$, plotted as a function of chlorophyll *a* concentration for the two wavelengths, 442 and 555 nm. Our data from Oceania and Polarstern are compared with regression lines from *Bricaud et al*. [1995] and *Bricaud et al*. [1998] shown as solid and dashed lines for 442 and 555 nm respectively.

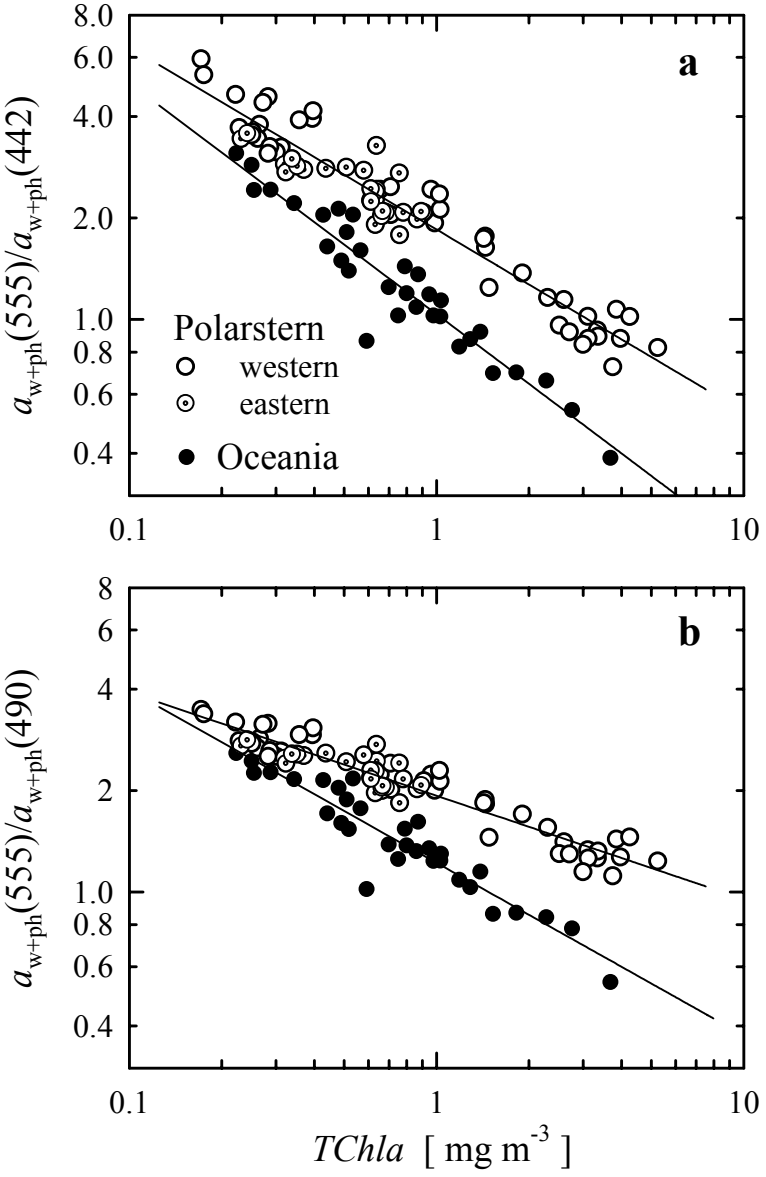

Figure 9. The absorption ratios $a_{w+ph}(555)/a_{w+ph}(442)$ and $a_{w+ph}(555)/a_{w+ph}(490)$ as a function of *TChla* from HPLC analysis. Data from Oceania and Polarstern are shown as solid and open symbols respectively.

The least-squares fits for Polarstern data:

$a_{w+ph}(555)/a_{w+ph}(442) = 1.848\ TChla^{-0.541}$; $r^2 = 0.93$; $n = 73$

$a_{w+ph}(555)/a_{w+ph}(490) = 1.931\ TChla^{-0.307}$; $r^2 = 0.91$; $n = 73$

The least-squares fits for Oceania data:

$a_{w+ph}(555)/a_{w+ph}(442) = 1.036\ TChla^{-0.687}$; $r^2 = 0.91$; $n = 31$

$a_{w+ph}(555)/a_{w+ph}(490) = 1.221\ TChla^{-0.512}$; $r^2 = 0.89$; $n = 31$

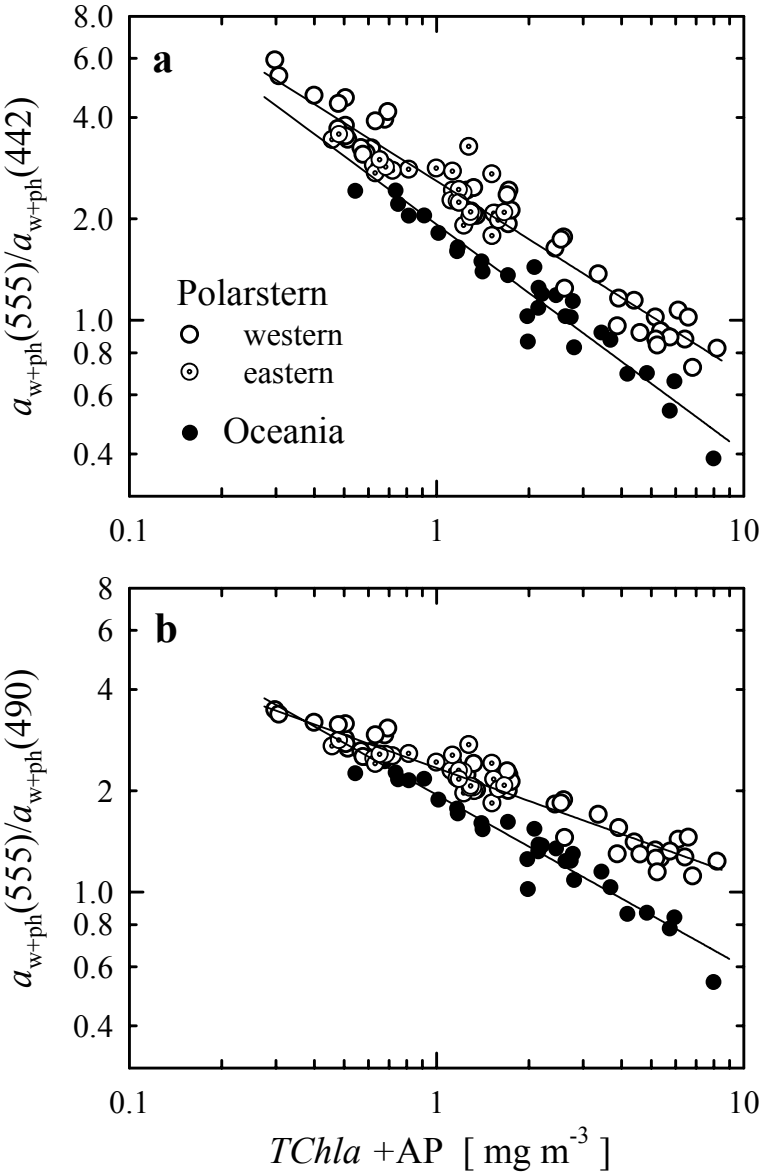

Figure 10. The absorption ratios $a_{w+ph}(555)/a_{w+ph}(442)$ and $a_{w+ph}(555)/a_{w+ph}(490)$ as a function of the sum of *TChla* and AP. Data from Oceania and Polarstern are shown as solid and open symbols respectively.

The least-squares fits for Polarstern data:

$a_{w+ph}(555)/a_{w+ph}(442) = 2.590\ (TChla + \mathrm{AP})^{-0.575}$; $r^2 = 0.94$; $n = 73$

$a_{w+ph}(555)/a_{w+ph}(490) = 2.338\ (TChla + \mathrm{AP})^{-0.326}$; $r^2 = 0.92$; $n = 73$

The least-squares fits for Oceania data:

$a_{w+ph}(555)/a_{w+ph}(442) = 1.924\ (TChla + \mathrm{AP})^{-0.676}$; $r^2 = 0.93$; $n = 31$

$a_{w+ph}(555)/a_{w+ph}(490) = 1.945\ (TChla + \mathrm{AP})^{-0.512}$; $r^2 = 0.93$; $n = 31$

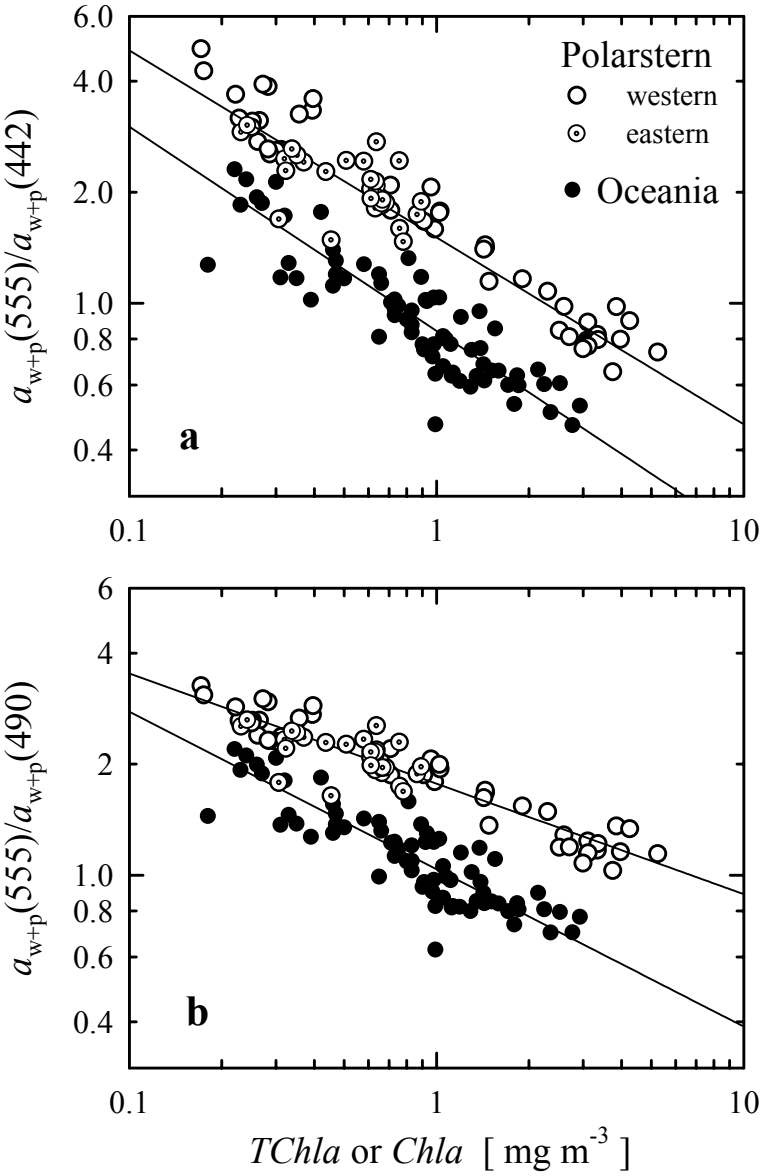

Figure 11. The absorption ratios $a_{w+p}(555)/a_{w+p}(442)$ and $a_{w+p}(555)/a_{w+p}(490)$ as a function of chlorophyll *a* concentration.

The least-squares fits for Polarstern data:

$a_{w+p}(555)/a_{w+p}(442) = 1.58\ TChla^{-0.51}$; $r^2 = 0.90$; $n = 73$

$a_{w+p}(555)/a_{w+p}(490) = 1.77\ TChla^{-0.3}$; $r^2 = 0.88$; $n = 73$

The least-squares fits for Oceania data:

$a_{w+p}(555)/a_{w+p}(442) = 0.83\ Chla^{-0.554}$; $r^2 = 0.82$; $n = 71$

$a_{w+p}(555)/a_{w+p}(490) = 1.04\ Chla^{-0.427}$; $r^2 = 0.79$; $n = 71$

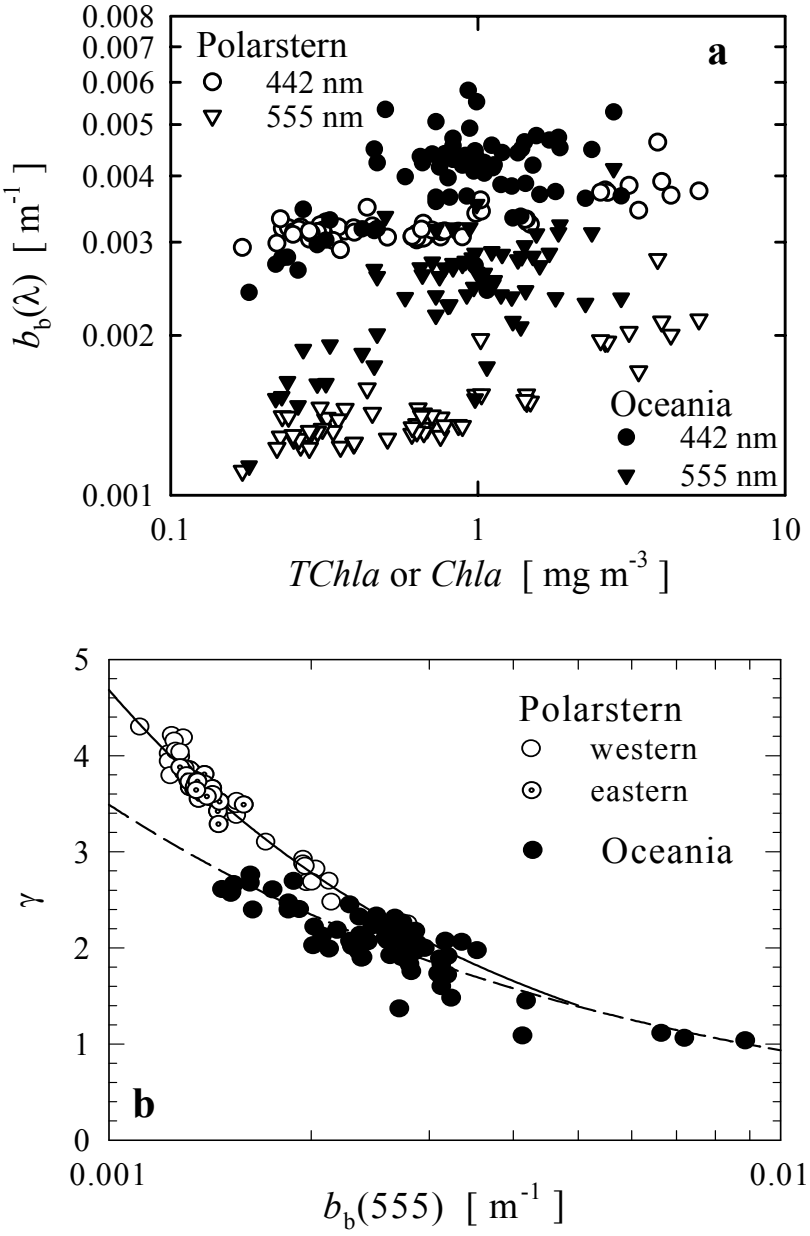

Figure 12. (a) The total backscattering coefficient b_b at 442 and 555 nm versus chlorophyll *a* concentration. (b) Slope parameter γ from equation 4 versus the total backscattering coefficient b_b at 555 nm.

The least-squares fit for Polarstern data:

$\gamma = 0.026\ b_b(555)^{-0.750}$; $r^2 = 0.95$; $n = 60$

The least-squares fit for Oceania data:

$\gamma = 0.067\ b_b\ (555)^{-0.572}$; $r^2 = 0.80$; $n = 73$

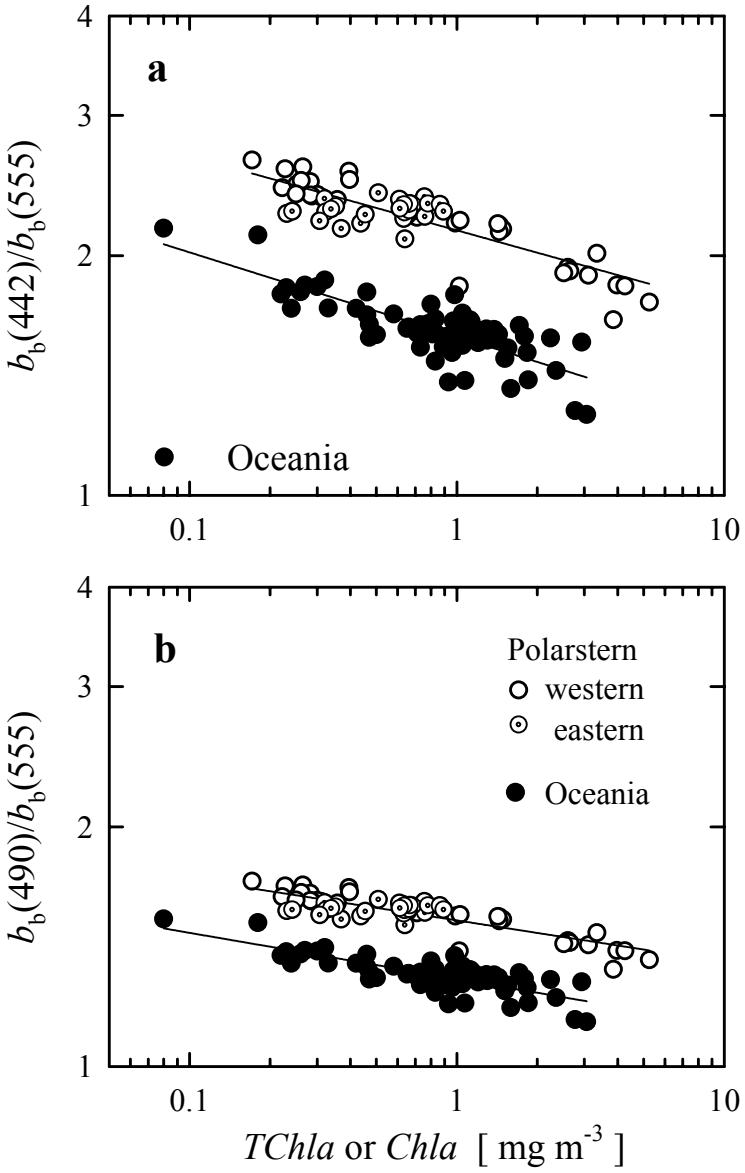

Figure 13. The backscattering ratios $b_b(442)/b_b(555)$ and $b_b(490)/b_b(555)$ as a function of chlorophyll *a* concentration.

The least-squares fits for Polarstern data:

$b_b(442)/b_b(555) = 2.152\ TChla^{-0.093}$; $r^2 = 0.70$; $n = 60$

$b_b(490)/b_b(555) = 1.526\ TChla^{-0.052}$; $r^2 = 0.73$; $n = 60$

The least-squares fits for Oceania data:

$b_b(442)/b_b(555) = 1.583\ Chla^{-0.106}$; $r^2 = 0.66$; $n = 73$

$b_b(490)/b_b(555) = 1.289\ Chla^{-0.058}$; $r^2 = 0.66$; $n = 73$

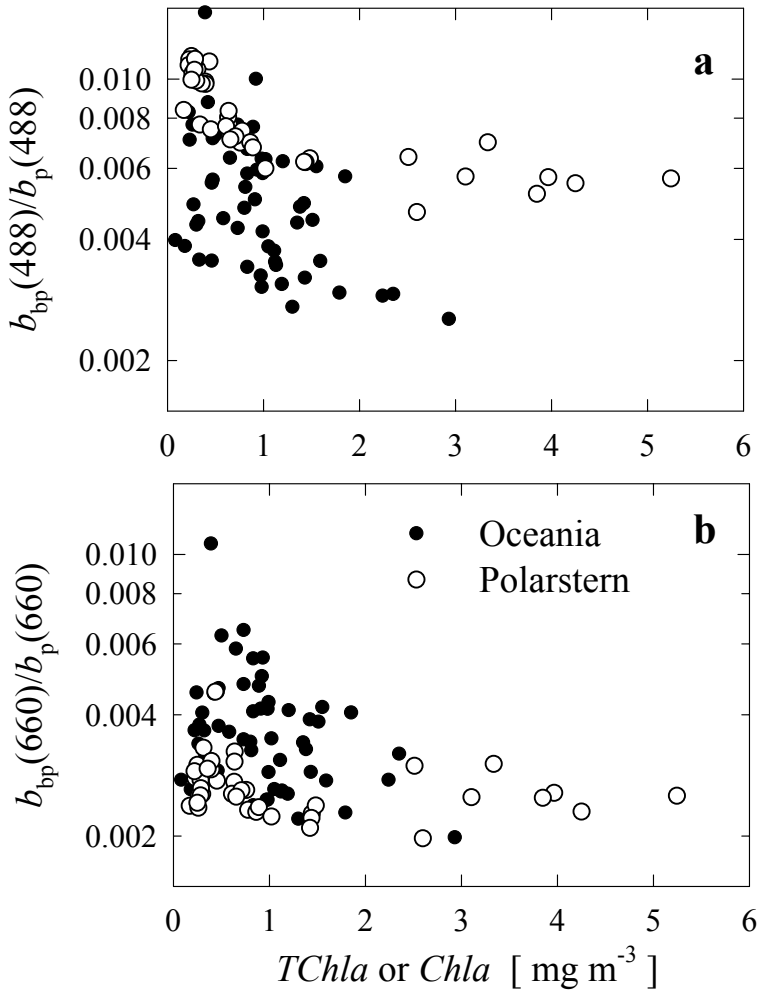

Figure 14. The particulate backscattering ratios (a) $b_{bp}(488)/b_p(488)$ and (b) $b_{bp}(660)/b_p(660)$ as a function of chlorophyll *a* concentration.

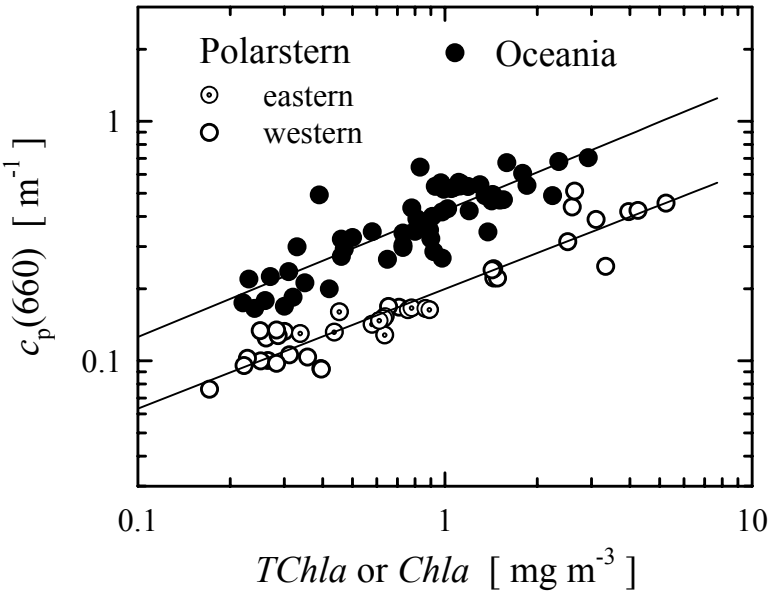

Figure 15. Relationships between the particulate beam attenuation coefficient at 660 nm, $c_p(660)$, and chlorophyll *a* concentration.

The least-squares fit for Polarstern data:

$c_p(660) = 0.1995\ TChla^{\,0.4995}$; $r^2 = 0.89$; $n = 42$

The least-squares fits for Oceania data:

$c_p(660) = 0.4244\ Chla^{\,0.5282}$; $r^2 = 0.72$; $n = 60$

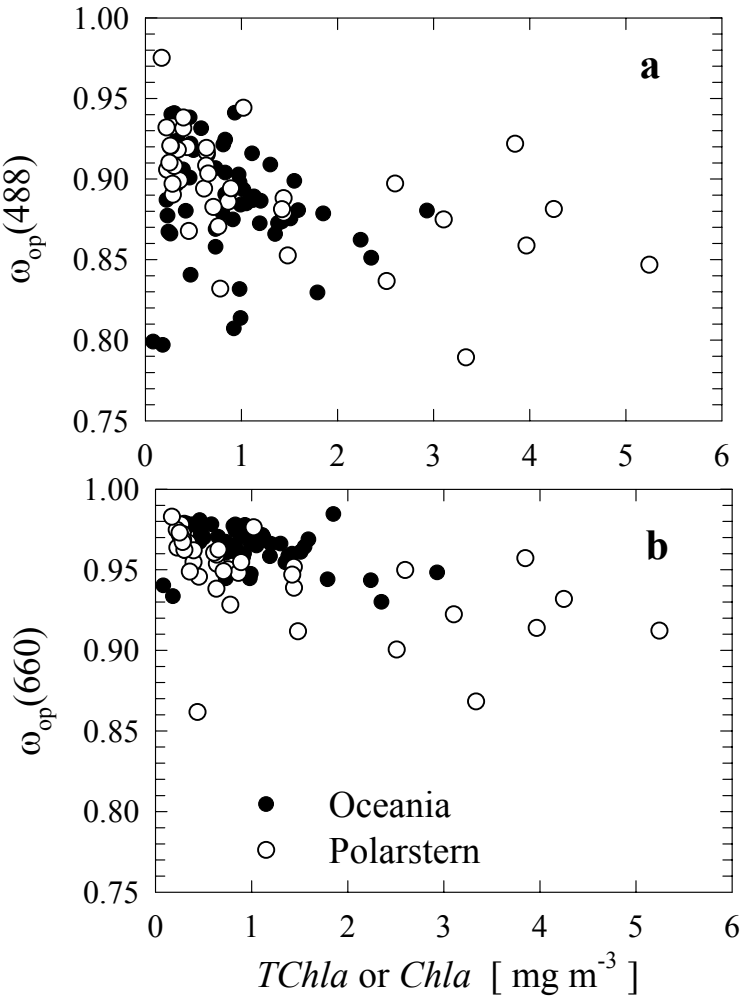

Figure 16. The single scattering albedo of particles, $\omega_{op}(488)$ and $\omega_{op}(660)$, as a function of chlorophyll *a* concentration.

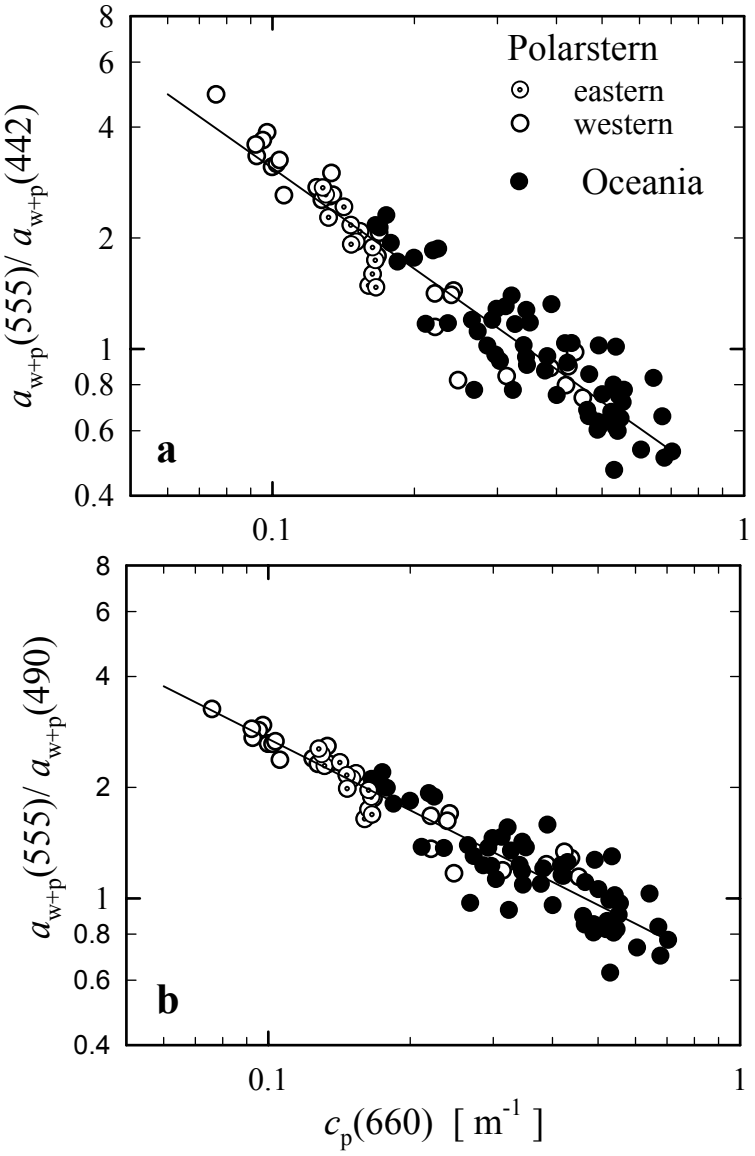

Figure 17. The absorption ratios $a_{w+p}(555)/a_{w+p}(442)$ and $a_{w+p}(555)/a_{w+p}(490)$ as a function of the particulate beam attenuation coefficient, $c_p(660)$.

The least-squares fits for Polarstern and Oceania data combined together:

$a_{w+p}(555)/a_{w+p}(442) = 0.6144\ c_p(660)^{-0.6441}$; $r^2 = 0.90$; $n = 102$

$a_{w+p}(555)/a_{w+p}(490) = 0.3834\ c_p(660)^{-0.9065}$; $r^2 = 0.89$; $n = 102$

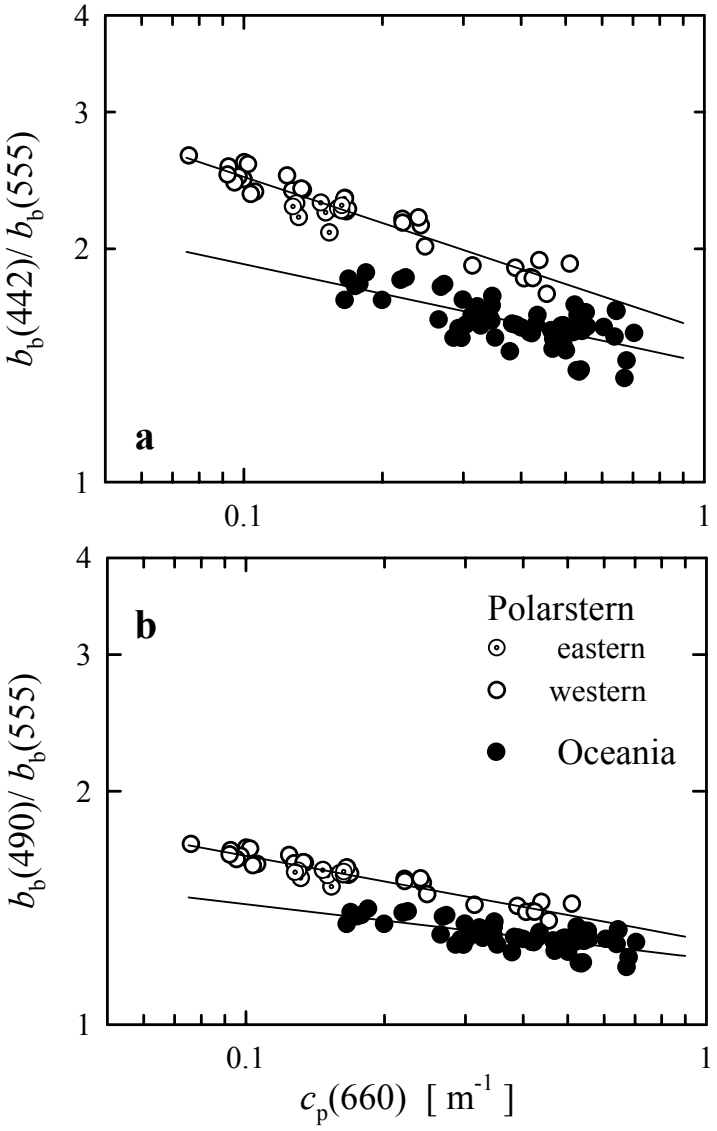

Figure 18. The backscattering ratios $b_b(442)/b_b(555)$ and $b_b(490)/b_b(555)$ as a function of the particulate beam attenuation coefficient, $c_p(660)$.

The least-squares fits for Polarstern data:

$b_b(442)/b_b(555) = 1.570\ c_p(660)^{-0.198}$; $r^2 = 0.91$; $n = 42$

$b_b(490)/b_b(555) = 1.283\ c_p(660)^{-0.109}$; $r^2 = 0.91$; $n = 42$

The least-squares fits for Oceania data:

$b_b(442)/b_b(555) = 1.426\ c_p(660)^{-0.127}$; $r^2 = 0.47$; $n = 60$

$b_b(490)/b_b(555) = 1.217\ c_p(660)^{-0.070}$; $r^2 = 0.47$; $n = 60$

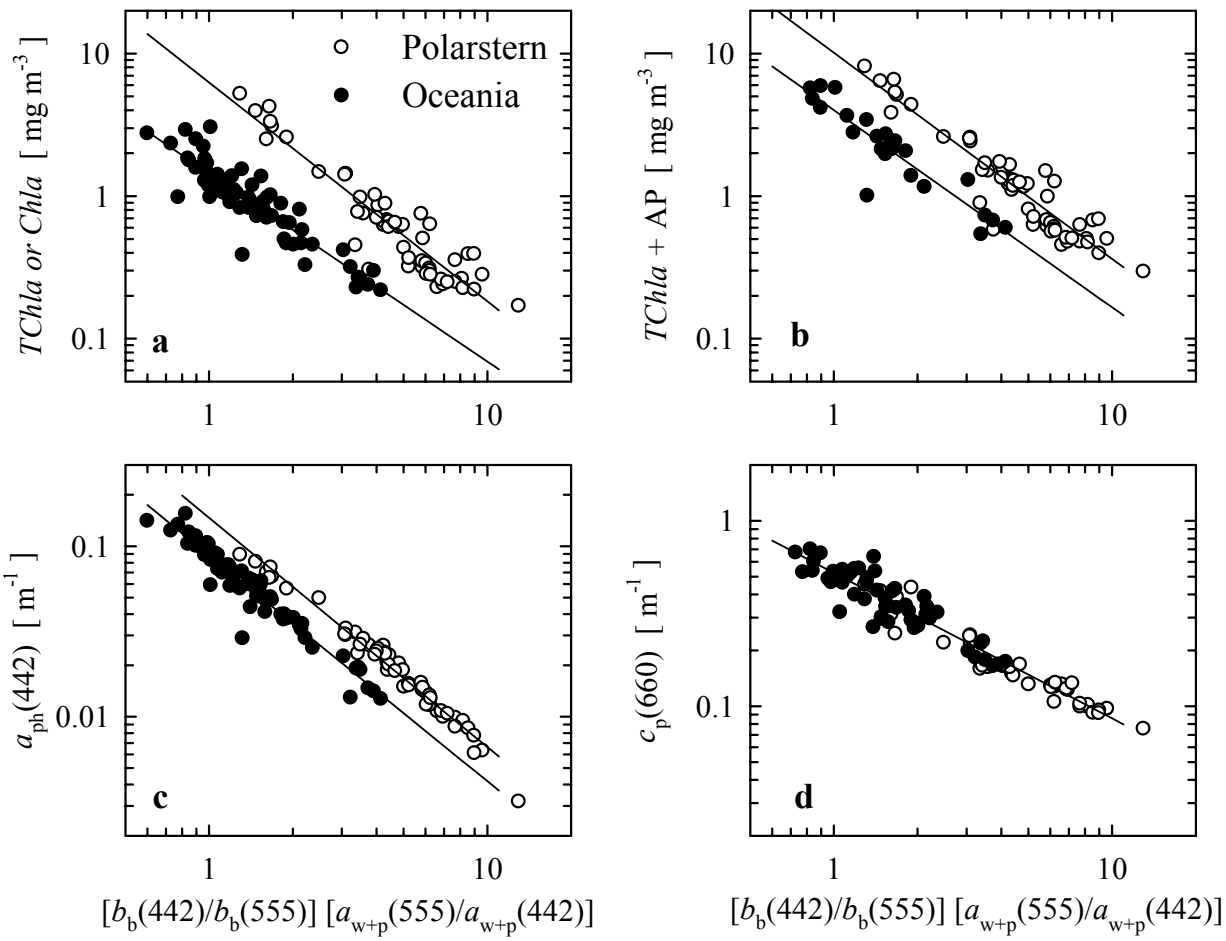

Figure 19. Relationships for (a) chlorophyll *a* concentration versus the product of the backscattering ratio and the absorption ratio, $R = [b_b(442)/b_b(555)]\,[a_{w+p}(555)/a_{w+p}(442)]$. This product is an approximation of the blue-to-green ratio of remote-sensing reflectance (see Eq. 1).
The least-squares fit for Polarstern data:
$TChla = 6.2517\ R^{-1.5349}$; $r^2 = 0.87$; $n = 42$
The least-squares fit for Oceania data:
$Chla = 1.4437\ R^{-1.32}$; $r^2 = 0.83$; $n = 60$

(b) As in (a) but for the sum of *TChla* and AP.
The least-squares fit for Polarstern data:
$(TChla+\mathrm{AP}) = 10.135\ R^{-1.4456}$; $r^2 = 0.88$; $n = 42$
The least-squares fit for Oceania data:
$(TChla + \mathrm{AP}) = 4.0145\ R^{-1.384}$; $r^2 = 0.85$; $n = 26$

(c) As in (a) but for the phytoplankton absorption coefficient at 442 nm, $a_{ph}(442)$.
The least-squares fit for Polarstern data:
$a_{ph}(442) = 0.1467\ R^{-1.3449}$; $r^2 = 0.98$; $n = 42$
The least-squares fit for Oceania data:
$a_{ph}(442) = 0.0885\ R^{-1.3257}$; $r^2 = 0.93$; $n = 50$

(d) As in (a) but for the particulate beam attenuation coefficient at 660 nm, $c_p(660)$.
The least-squares fits for Polarstern and Oceania data combined together:
$c_p(660) = 0.5227\ R^{-0.784}$; $r^2 = 0.93$; $n = 92$

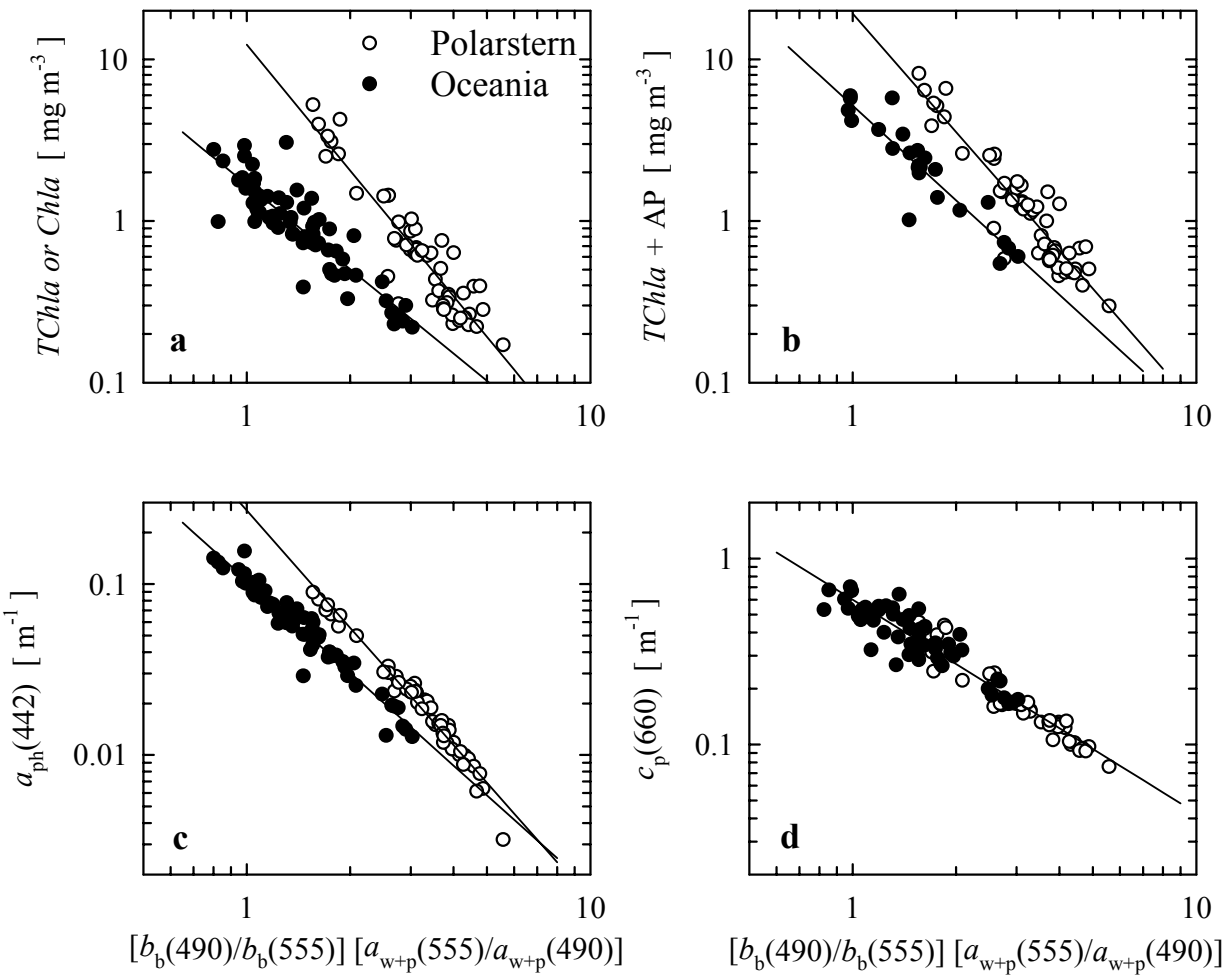

Figure 20. Relationships for (a) chlorophyll *a* concentration versus the product of the backscattering ratio and the absorption ratio, $R = [b_b(490)/b_b(555)]\,[a_{w+p}(555)/a_{w+p}(490)]$. This product is an approximation of the blue-to-green ratio of remote-sensing reflectance (see Eq. 1).

The least-squares fit for Polarstern data:
$TChla = 12.318\ R^{-2.5844}$; $r^2 = 0.86$; $n = 42$
The least-squares fit for Oceania data:
$Chla = 1.6766\ R^{-1.7356}$; $r^2 = 0.79$; $n = 60$

(b) As in (a) but for the sum of *TChla* and AP.
The least-squares fit for Polarstern data:
$(TChla + AP) = 19.189\ R^{-2.4337}$; $r^2 = 0.86$; n = 42

The least-squares fit for Oceania data:
($TChla$ + AP) = 5.1763 $R^{-1.9446}$; r^2 = 0.85; n = 26

(c) As in (a) but for the phytoplankton absorption coefficient at 442 nm, $a_{ph}(442)$.
The least-squares fit for Polarstern data:
$a_{ph}(442) = 0.2696\ R^{-2.2766}$; r^2 = 0.97; n = 42
The least-squares fit for Oceania data:
$a_{ph}(442) = 0.1054\ R^{-1.8014}$; r^2 = 0.95; n = 50

(d) As in (a) but for the particulate beam attenuation coefficient at 660 nm, $c_p(660)$.
The least-squares fits for Polarstern and Oceania data combined together:
$c_p(660) = 0.5999\ R^{-1.1475}$; r^2 = 0.92; n = 92